

Deep-learning-based sub-seasonal precipitation and streamflow ensemble forecasting over the source region of the Yangtze River

Ningpeng Dong, Haoran Hao, Mingxiang Yang, Jianhui Wei, Shiqin Xu, Harald Kunstmann

Angaben zur Veröffentlichung / Publication details:

Dong, Ningpeng, Haoran Hao, Mingxiang Yang, Jianhui Wei, Shiqin Xu, and Harald Kunstmann. 2025. "Deep-learning-based sub-seasonal precipitation and streamflow ensemble forecasting over the source region of the Yangtze River." *Hydrology and Earth System Sciences* 29 (8): 2023–42. <https://doi.org/10.5194/hess-29-2023-2025>.



Deep-learning-based sub-seasonal precipitation and streamflow ensemble forecasting over the source region of the Yangtze River

Ningpeng Dong¹, Haoran Hao^{2,1}, Mingxiang Yang¹, Jianhui Wei³, Shiqin Xu⁴, and Harald Kunstmann^{3,5,6}

¹State Key Laboratory of Simulation and Regulation of Water Cycle in River Basin, China Institute of Water Resources and Hydropower Research, Beijing, China

²State Key Laboratory of Hydraulic Engineering Intelligent Construction and Operation, Tianjin University, Tianjin, China

³Institute of Meteorology and Climate Research (IMKIFU), Karlsruhe Institute of Technology, Campus Alpin, Garmisch-Partenkirchen, Germany

⁴Hydrology, Agriculture and Land Observation (HALO) Laboratory, King Abdullah University of Science and Technology, Thuwal, Saudi Arabia

⁵Institute of Geography, University of Augsburg, Augsburg, Germany

⁶Centre for Climate Resilience, University of Augsburg, Augsburg, Germany

Correspondence: Ningpeng Dong (dongnp@iwhr.com) and Haoran Hao (1020205041@tju.edu.cn)

Received: 9 July 2024 – Discussion started: 29 July 2024

Revised: 1 November 2024 – Accepted: 5 February 2025 – Published: 22 April 2025

Abstract. Hydrometeorological forecasting is crucial for managing water resources and mitigating the impacts of hydrological extremes. At sub-seasonal scales, readily available hydrometeorological forecast products often exhibit large uncertainties and insufficient accuracies to support decision-making. We propose a deep-learning-based modelling framework for sub-seasonal joint precipitation and streamflow ensemble forecasts for a lead time of up to 30 d. This is achieved by coupling (1) an ensemble of enhanced convolutional neural network (CNN) models with ResNet blocks and a specialized loss function for statistically downscaling of European Centre for Medium-Range Forecasts (ECMWF) ensemble precipitation forecasts to (2) a hybrid hydrologic model integrating the conceptual Xin'anjiang model (XAJ) and the long short-term memory network (LSTM) for ensemble streamflow forecasting (XAJ-LSTM). Applying the modelling framework to the source region of the Yangtze River Basin, results indicate that the CNN-based downscaling model exhibits $\sim 34\%$ and $\sim 26\%$ less root mean squared error (RMSE) than the raw ECMWF forecasts and the quantile mapping (QM) forecasts, respectively, averaged over the 30 d lead time. Similarly, the CNN achieves approximately 6% and 10% lower RMSE than raw forecasts and QM for heavy precipitation events. Using these precipitation forecasts as meteorological forcing for the hy-

brid XAJ-LSTM hydrologic model, we found that forecasted streamflow and flood peaks driven by CNN-based precipitation forecasts have 16%–33% lower relative errors and 20%–31% lower RMSE compared to those driven by raw forecasts. However, the standalone XAJ model shows only marginal improvements with the same enhanced precipitation forecasts. This highlights the importance of understanding the effectiveness of the hydrologic model as part of the sub-seasonal hydrometeorological modelling chain. Our study is expected to provide implications for leveraging advanced AI techniques to enhance sub-seasonal hydrometeorological forecasting accuracy and operational efficiency for effective water resources management and disaster preparedness.

1 Introduction

In past decades, the frequency and intensity of extreme precipitation events have been increasing in many areas as global warming continues, thereby amplifying the potential for hazards of extreme weather and hydrologic events (Wei et al., 2018; Yuan et al., 2018; Wang et al., 2019; Zhu et al., 2020). Hydrological forecasting has become critically important for managing water resources and mitigating the impacts

of these extreme weather and hydrologic events (Robertson and Wang, 2013; Liu et al., 2020; Jiang et al., 2022). Traditional hydrological forecasts, which do not integrate sub-seasonal meteorological forecasts, often provide insufficient lead times for decision-making on flood control, agricultural planning, and ecological preservation efforts (de Andrade et al., 2021; Bierkens, 2015; Jaun et al., 2008). Integrating both meteorological and hydrological forecasts at sub-seasonal scales is therefore essential to extend lead times, thereby improving water resources management and disaster preparedness over a longer term (Yuan et al., 2016; Cloke and Pappenberger, 2009; Liang et al., 2018; Vigaud et al., 2019; Zhu et al., 2019).

Advancements in numerical weather prediction (NWP) models, such as the European Centre for Medium-Range Forecasts (ECMWF) Integrated Forecasting System (IFS) and the NCEP Global Forecast System (GFS), have greatly improved the accuracy of sub-seasonal weather forecasting (Yuan et al., 2011; Bauer et al., 2015; Brotzge et al., 2023). However, these global models often suffer from relatively coarse resolutions and generalized parameterizations that may not be suitable for regional-scale and local-scale forecasts (Dehshiri and Firoozabadi, 2023; Singhal et al., 2023). Dynamic downscaling, such as that performed by the Weather Research and Forecasting (WRF) model, translates larger-scale atmospheric trends captured by global climate models (GCMs) into fine-scale regional details that reflect local geographic and climatic factors (Merino et al., 2022; Noonii et al., 2022; Maraun et al., 2010). For instance, recent studies by Gao et al. (2022) and Srivastava et al. (2023) demonstrate the effectiveness of WRF in enhancing the accuracy of precipitation forecasts and capturing the dynamics of severe weather events. Despite these advantages, dynamic downscaling often requires extensive computational resources especially for sub-seasonal scales, and can be sensitive to the quality of input data. Furthermore, the process is constrained by the physical parameterizations that may not always accurately represent localized meteorological conditions, a concern that is increasingly critical under changing climatic conditions (Di Luca et al., 2015; Shi, 2020; Xu et al., 2015).

Statistical downscaling techniques, which have been used to relate the larger-scale meteorological patterns to local-scale weather, offer a different approach (Tabari et al., 2021; Zhang et al., 2022a; Michalek et al., 2024). Traditional statistical downscaling methods such as quantile mapping have proven effective in reducing the systematic bias of precipitation forecasts with relatively simple inputs (Vrac and Friederichs, 2015). On the other hand, forecasting weather and predicting climate using machine learning, especially deep learning (DL), has recently become a hot topic. A common approach for this purpose is to use preceding predictors from observational or reanalysis data to forecast subsequent predictands (Weyn et al., 2021; Xie et al., 2023; Ham et al., 2019; Ling et al., 2022). An alternative method

involves post-processing dynamical forecasts. For instance, Cho et al. (2020) applied machine learning techniques, including random forests and support vector machines, to develop statistical relationships for temperature adjustments. Similarly, Kim et al. (2021) utilized long short-term memory (LSTM) networks to correct bias in the amplitude and phase of the Madden–Julian Oscillation. More recently, deep learning models such as convolutional neural networks (CNNs) have been reported able to more effectively reduce the total bias of meteorological forecasts due to their ability to learn multi-dimensional representations of data features (Vandal et al., 2019; Sachindra et al., 2018; Jiang et al., 2024; Li et al., 2022). For example, Lagerquist et al. (2019) used a CNN to identify fronts in gridded data for spatially explicit prediction of synoptic-scale fronts.

Despite general improvements of forecasts, these DL-based models tend to smooth the extreme precipitation at sub-seasonal scales (Baño-Medina et al., 2021; Kim et al., 2022), likely due to insufficient heavy precipitation samples (Chen and Wang, 2022). Many studies have since introduced more recent variants of CNNs including the U-shaped U-Net (Han et al., 2021; Horat and Lerch, 2024; Ni et al., 2023) and SmaAt-UNet (Li et al., 2024a), or coupled standard CNNs with different structures, such as auto-encoders (Ling et al., 2022a) and LSTM (Ling et al., 2022b). In particular, the residual network, ResNet, has been introduced in sub-seasonal forecast correction, which shows the potential of mitigating the vanishing gradient issue by introducing the residual paths (Jin et al., 2022; Nie and Sun, 2024). Others have attempted to introduce specialized loss functions to balance heavy and light rains, such as the exponentially weighted mean squared error (Ebert-Uphoff and Hilburn, 2020) and Dice loss (You et al., 2023). However, these new developments have not been sufficiently examined for sub-seasonal forecasts.

Other state-of-the-art forms of deep learning for weather forecasts include fully DL-based models, such as Pangu (Bi et al., 2023) and GraphCast (Lam et al., 2023), which are reported able to achieve forecast skills comparable to numerical weather prediction systems. While these models may appear quite different from statistical post-processing deep learning models, some argue that these models act more as post-processing tools rather than realistic simulators of the atmosphere due to the lack of physical fidelity and consistency (Bonavita, 2024). Although not the primary focus of this paper, this calls attention to the scientific community to critically evaluate and differentiate between the capabilities and applications of fully DL-based models and DL models designed for post-processing.

In addition to meteorological forecasts, sub-seasonal streamflow forecasts are crucial because streamflow at these timescales is directly related to the onset and progression of flooding and drought events. To translate meteorological predictions to streamflow forecasts, both physics-based and data-driven hydrologic forecasting models are widely

used. Physics-based models, such as the lumped Xin'anjiang model, HBV model, and the distributed CLHMS and VIC models, make predictions by interpreting detailed physical processes (Gassman et al., 2014; Dong et al., 2022, 2023). Data-driven models were also developed to perform rainfall-runoff modelling and forecasts by learning from big data (Kisi, 2007; Adnan et al., 2019) and have been reported to outperform the well-calibrated physics-based models (Kratzert et al., 2019). It is noteworthy that both models are embedded with uncertainties. Physics-based models may produce inaccurate simulations due to simplified representations of hydrologic processes, and data-driven models may perform less effectively in extrapolation beyond the range of the training data (Addor et al., 2020). By integrating the strengths of both approaches, recent studies have attempted to establish a hybrid model with a higher predictive performance than the physical model alone (Liu et al., 2022; Abraham et al., 2012; Raftery et al., 2005; Yang et al., 2020). For example, Humphrey et al. (2016) combined a Bayesian neural network (BNN) with the traditional GR4J model and achieved improved forecast accuracy compared to using either the BNN or GR4J alone. However, the role of such models as part of the hydrometeorological modelling chain in producing reliable streamflow forecasts has not been well examined at sub-seasonal scales. For example, Crochemore et al. (2016) and Valdez et al. (2022) suggested that the relationship between the accuracy of precipitation forecasts and the corresponding streamflow forecasts is not necessarily straightforward. An ensemble approach with DL models also shows promising results (Ferranti et al., 2018; Bremnes, 2020; Balint et al., 2006; Cloke and Pappenberger, 2009; Scheuerer and Hamill, 2015; Taillardat et al., 2016) that require further investigation.

The above considerations are particularly relevant for the source region (SR) of the Yangtze River Basin, which is historically susceptible to extensive flooding and droughts that affect thousands of kilometres downstream (Sun et al., 2016). Aiming at enhancing sub-seasonal hydrometeorological forecasts for the wet season in this area, we start by addressing the following questions:

1. How effectively can CNN architectures with recent extensions improve the sub-seasonal precipitation forecasts compared to traditional statistically downscaling models?
2. How effectively can AI-assisted hydrologic models convert more accurate sub-seasonal precipitation forecasts into more accurate streamflow forecasts compared to traditional conceptual hydrologic models?

Specifically, this study investigates sub-seasonal precipitation and streamflow ensemble forecast skills for up to 30 d ahead with deep learning models, which integrates enhanced CNN models with ResNet blocks and specialized loss functions for post-processing the ensemble ECMWF forecasts

with a hybrid hydrologic model of the Xin'anjiang model (XAJ) and the long short-term memory network (LSTM) for streamflow forecasting. Our approaches and findings are expected to provide implications for operational hydrometeorological forecasts in the SR and also similar basins worldwide.

2 Study area and data

2.1 Study area

The source region (SR) of the Yangtze River Basin is located on the eastern edge of the Tibetan Plateau, between 26–36° N and 90–101° E, as shown in Fig. 1. The region serves as a crucial transitional area from highland mountains to plains in southern China, with the surface elevation decreasing from over 6000 m in the north to just over 2500 m in the south. The climate of the region is subject to both plateau and subtropical monsoon climates, with annual precipitation ranging from 280 to 760 mm. The SR has a significant impact on the utilization of water resources in the Yangtze River Basin and southwest China (Hao et al., 2024). The controlling hydrologic station of the SR is Shigu station (Fig. 1), which has a mean annual streamflow of around $1300 \text{ m}^3 \text{ s}^{-1}$, accounting for 5 % of the total water resources of the Yangtze River Basin.

The SR spans a large north–south range, with the northern region deep in the Tibetan Plateau and dominated by a plateau monsoon climate and the southern region characterized by low hills and a subtropical monsoon climate. These contrasting environments suggest different runoff generation mechanisms between the two regions. To ensure the accuracy of streamflow simulations at Shigu, we therefore divided the SR into two sub-basins (i.e. northern and southern basins in Fig. 1) for hydrologic modelling in Sect. 3.4.

2.2 Data sources

2.2.1 Observed precipitation and temperature

To train the forecast models and evaluate the accuracy of forecasts, this study employs the 0.25° daily precipitation and temperature grid dataset (CN05.1), released by the National Meteorological Information Center, as the reference observed data. This dataset is produced by interpolating precipitation and temperature data from over 2000 meteorological stations across the country and covers the period from 1961 to 2022.

2.2.2 ECMWF sub-seasonal reforecast data

The European Centre for Medium-Range Weather Forecasts (ECMWF) offers a sub-seasonal forecast service designed to bridge the gap between short-range weather predictions and long-term climate outlooks. This service focuses on predicting atmospheric and oceanic conditions over the next 2 to 6

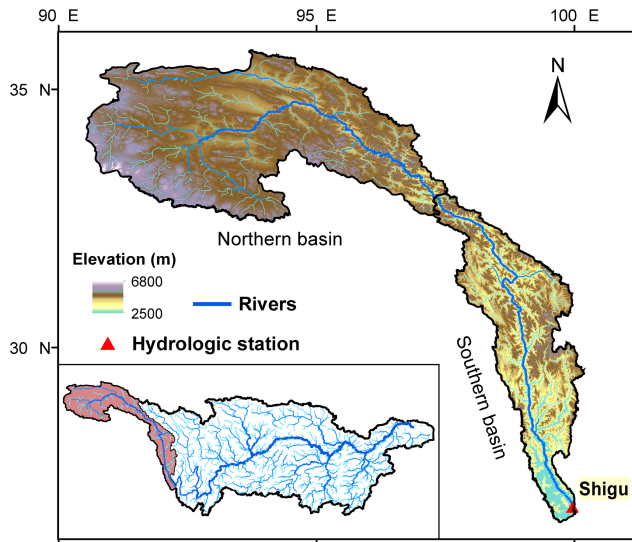


Figure 1. The source region of the Yangtze River Basin and its location in the Yangtze River Basin.

weeks, providing valuable information for a variety of applications such as water resources management and disaster preparedness. In this study, we collect the ECMWF Sub-seasonal to Seasonal (S2S) daily reforecast data for a lead time of 30 d initialized on 35 dates during the wet season (between May and August) per year during 2002–2019. The forecasted variables used in this study include precipitation and convective precipitation at the land surface and temperature, wind components, geopotential heights, and specific humidity at 200, 500, and 850 hPa pressure levels. All of these variables are at a spatial resolution of 1.5° .

2.2.3 Observed streamflow

To calibrate the hybrid hydrologic model and evaluate the hydrologic forecasts, the daily streamflow data of Shigu station are collected for 1981–2019.

3 Methods

3.1 Overview

The presented sub-seasonal hydrometeorological forecasting framework aims to improve the daily precipitation forecasts and the corresponding streamflow forecasts at the Shigu hydrologic station during the wet season (May to August) for a lead time up to 30 d. We first employ all 10 ensemble members from the ECMWF S2S gridded sub-seasonal precipitation reforecast dataset for the next 30 d as raw forecasts, denoted as EC. An ensemble of enhanced CNN models with ResNet blocks and a specialized loss function is established to statistically downscale and bias-correct each ensemble member of the 1.5° EC raw precipitation forecasts to 0.25°

grid resolution, with its post-processed forecast denoted EC-CNN (Sect. 3.2.1). The quantile mapping (QM) serves as a benchmark for comparison, with its post-processed forecast denoted EC-QM (Sect. 3.2.2).

These three gridded ensemble precipitation forecasts (EC, EC-QM, and EC-CNN), along with ECMWF gridded sub-seasonal daily temperature forecasts corrected by the delta method (Sect. 3.3), are employed to drive two lumped hydrologic models to produce the daily streamflow forecasts for lead times of 1–30 d. All these gridded forecasts are areal-averaged over the two sub-basins of the SR (Fig. 1) before being input to the lumped hydrologic models. The first hydrologic model is a standalone XAJ model (Sect. 3.4.1), and the second model is a hybrid model that integrates the conceptual XAJ model and the LSTM (hereinafter XAJ-LSTM) (Sect. 3.4.2 and 3.4.3). The streamflow and flood forecasts of XAJ-LSTM and standalone XAJ driven by EC-CNN forecasts are then quantitatively evaluated against those driven by EC and EC-QM forecasts.

The evaluation metrics include deterministic metrics of root mean squared error (RMSE), relative error (RE), and the Nash–Sutcliffe efficiency (NSE) for the ensemble mean and probabilistic metrics of continuous ranked probability score (CRPS) for a total of 10 ensemble members (Sect. 3.5). A detailed workflow of this study is presented in Fig. 2.

3.2 Statistically downscaling of ensemble precipitation forecasts

3.2.1 Enhanced convolutional neural network

An ensemble of enhanced CNN models with ResNet blocks and a specialized loss function is established to learn the spatially dependent relationship between fine-resolution local precipitation and coarse-resolution predictors from surrounding regions. Specifically, it downscales a total of 10 ensemble members of the ECMWF S2S reforecasts from a 1.5° resolution to a 0.25° resolution, using the CN05.1 reference precipitation dataset. The model takes spatially distributed inputs of 19 predictors, including the surface elevation, convective precipitation, and total precipitation at the surface level and U and V wind components, specific humidity, temperature, and geopotential height at 200, 500, 850 hPa pressure levels, from ECMWF forecasts. These inputs cover a 3×3 area of coarse grid cells at 1.5° resolution, centred around the target fine grid cell at 0.25° resolution. Due to the square-shaped input structure of the CNN model, some ECMWF data from outside the basin boundary are included in the input. For the outputs, the predictand is the daily precipitation at a spatial resolution of 0.25° , and the CNN loops over each fine-resolution grid cell (0.25°) within the basin boundary, thereby generating a high-resolution precipitation forecast for the entire SR. Figure 2 presents the model structure, which primarily consists of convolutional layers, em-

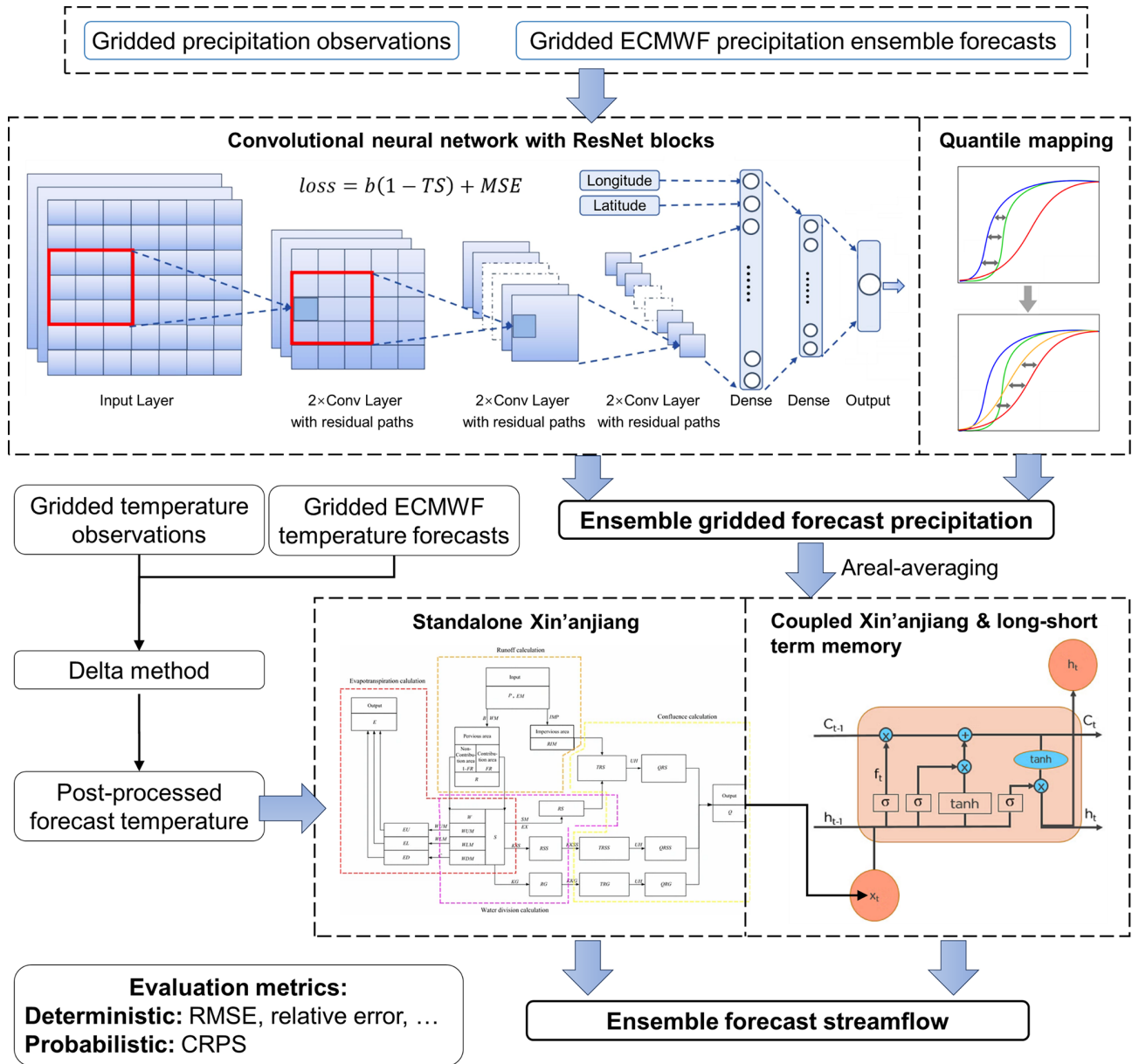


Figure 2. The workflow of this study.

bedding layers, fully connected layers, and residual paths. More details on the model structure are described as follows.

1. Inputs to the network are predictors from a 3×3 grid patch (1.5° resolution) centred on the target grid cell (0.25° resolution). This patch includes a total of 19 meteorological variables, resulting in input arrays with sizes of $19 \times 3 \times 3$. The spatial dimension of 3×3 is selected because it shows the best performance among four candidates of 1×1 , 3×3 , 5×5 , and 7×7 .
2. The model includes three ResNet blocks, with each block containing two convolutional layers with 3×3 kernels and feature maps of sizes 64, 32, and 16, re-

spectively. Such blocks mitigate the vanishing gradient problem and improve computational efficiency for a moderately deep learning model as in our study by allowing the gradient to bypass certain layers. For each convolutional layer, the convolution procedure involves moving the kernels along the input spatial fields, with the dot product calculated between the inputs and the kernels to capture spatial features. The l th feature map of the current convolutional layer X_n^l is computed from the previous layer X_{n-1} with K feature maps through

the convolutional operation as follows:

$$X_n^l = \text{ELU} \left(b_n^l + \sum_{k=1}^K W_n^{k,l} * X_{n-1}^k \right), \quad (1)$$

where $W_n^{k,l}$ denotes the convolutional kernels, b_n^l is the bias for the l th feature map, and the symbol $*$ denotes two-dimensional convolution. Here, we employ exponential linear units (ELUs) as the activation function, i.e.

$$f(x) = \begin{cases} x & x > 0 \\ a(e^x - 1) & x \leq 0 \end{cases}, \quad (2)$$

where a is a hyperparameter to be estimated, and x is the input to the ELU function.

3. To address spatial heterogeneity, embedding layers are introduced to convert the coordinate indices into latitude and longitude decimals (Rasp and Lerch, 2018). The outputs from these embedding layers are merged with the flattened outputs from the ResNet blocks, and these combined data are then fed into two fully connected layers before the output layer.

The Adam optimizer is used to train the CNN model with an early stopping technique to avoid overfitting. Specifically, to account for the small number of extreme precipitation samples, a specialized loss function that combines the threat score (TS) and mean squared error (MSE) is used in this study, i.e.

$$\text{loss} = b(1 - \text{TS}) + \text{MSE}$$

$$\text{MSE} = \frac{1}{N} \sum_{i=1}^N (F_i - O_i)^2$$

$$\text{TS} = \frac{H}{H + F + M}, \quad (3)$$

where b represents the weight of extreme precipitation in model training. F_i is the i th forecast data, O_i is the i th observation data, and N is the number of data. Meanwhile, H , F , and M represent the hits, false alarms and misses, respectively. Note that the categorical indices used for calculating TS are discrete, which is not well suited for training deep learning models. Thus, the differentiable formulations proposed by Larraondo et al. (2020) and Lyu et al. (2023) are utilized in this study, i.e.

$$H = (O > \alpha) \odot \text{sigmoid}(F - \alpha) \quad (4)$$

$$F = (O < \alpha) \odot \text{sigmoid}(F - \alpha) \quad (5)$$

$$M = (O > \alpha) \odot \text{sigmoid}(-F - \alpha) \quad (6)$$

$$\text{sigmoid}(x) = \frac{1}{1 + e^{-ax}}, \quad (7)$$

in which \odot means element-wise multiplication, and the $(O > \alpha)$ and $(O < \alpha)$ are logical operations, which are

1 and 0 when the statement are true and false, respectively. α is the precipitation threshold that corresponds to the 90th percentile of observed precipitation of each grid cell for 2002–2019. The logical operations towards the F (forecast) term are substituted with a sigmoid function, which represents a smooth transition between the Boolean values at the threshold point. In the above expressions, a and b are hyperparameters that are determined following Lyu et al. (2023); see Table S1 in the Supplement for detailed values.

Another approach for improving extreme precipitation forecasts is to manually increase the number of heavy precipitation events within the training datasets. This approach is eventually not adopted in our study because it is found to degrade the sub-seasonal forecast accuracy of light precipitation events while not improving the accuracy of heavy precipitation events over the SR region (results not shown). A possible reason is that by doing so artificial disruptions are brought into the distribution of precipitation samples, which could possibly impair the generalization capability of models (You et al., 2023).

3.2.2 Quantile mapping

Quantile mapping is a widely used post-processing technique and is able to effectively enhancing quantitative precipitation forecasts at the sub-seasonal timescale (Li et al., 2024). Therefore, the current study adopts QM as a benchmark to evaluate the proposed CNN-based model.

We implement QM using a non-parametric approach that adjusts the quantiles of the forecasted and observed data without assuming a specific distribution. Specifically, the empirical cumulative distribution functions (CDFs) of observed and forecasted daily precipitation are built respectively, and each percentile of the forecasted data is adjusted to match the corresponding percentile in the observed data. Dry days with a precipitation amount less than 0.1 mm are excluded from the derivation of CDFs (Gudmundsson et al., 2012). To match the 1.5° forecast resolution with the 0.25° reference dataset resolution, the empirical CDFs are established separately for each 0.25° grid from the corresponding 1.5° forecast grid cell. Manzanos et al. (2018), Cannon et al. (2015), and other studies have indicated the effectiveness of this implementation in improving the overall precipitation forecasts.

Here, the period from 2002–2015 is used to estimate the empirical CDFs, and these CDFs are then used to correct the EC forecasts in the test period of 2016–2019:

$$\tilde{p}_{\text{QM}} = O^{-1} [F(p_{\text{EC}})], \quad (8)$$

where \tilde{p}_{QM} and p_{EC} are the QM-based precipitation forecasts and the ECMWF raw precipitation forecasts, respectively. The QM is constructed separately for each lead time to account for forecast bias variations across different lead

times. For each lead time, a single model is applied across all months, which is aligned with the structure of the CNN model built in this study.

3.3 Bias correction of temperature forecasts

In this study, we apply the widely used delta method to correct the ECMWF temperature forecasts for lead times of 1–30 d. We calculate the difference between observed and forecast temperature (i.e. the delta) for each lead time during May and August of 2002–2015 as a calibration period and then apply a single delta model for each lead time to the forecast temperature during May and August of 2016–2019 as a validation period. Given that temperature is not the main focus of the paper, in addition to the fact that temperature forecasts generally have less bias and much less hydrologic impact than precipitation forecasts (as discussed in Sect. 5.3), relevant evaluation results are provided in Sect. S1 in the Supplement.

3.4 Hybrid hydrologic model of XAJ-LSTM

3.4.1 Xin'anjiang model

The XAJ model is a conceptual hydrological model (Zhao, 1992), which has been widely used to generate flood forecasts for humid and semi-humid regions of China. The lumped XAJ model consists of the evapotranspiration module, the runoff generation module, the runoff partition module, and the runoff routing module (Hu et al., 2005). In this study, a modified version of XAJ model with snow accumulation and melting mechanisms is employed to simulate and forecast the daily streamflow of the SR at the sub-seasonal scale, which shows satisfactory accuracies for basins with snowmelt runoff in our previous study (Tan et al., 2023).

3.4.2 Long short-term memory network

In this study, the LSTM model is employed as part of the modelling chain to simulate and predict the sub-seasonal streamflow. LSTMs have memory cells that are analogous to the states of a traditional dynamical system model (Kratzert et al., 2018), which make them practicable for simulating natural hydrologic systems. Compared with other types of recurrent NNs (RNNs), LSTMs perform better in coping with exploding and vanishing gradients, which enables them to learn the long-term dependencies between input and output arrays (Zhang et al., 2022b). This is particularly desirable for modelling hydrological processes that have relatively long-time dependencies as compared with input-driven processes such as direct surface runoff. For example, Kratzert et al. (2018, 2019) applied LSTMs to hydrologic modelling and show that the internal memory states of the network are highly correlated with observed snow and soil moisture states, even if no snow or soil moisture data were input to the models during training. This model feature allows accurate sub-seasonal

hydrologic simulations in the SR where there is snow accumulation around the winter and spring.

3.4.3 Model integration

The XAJ model employs daily precipitation and temperature of the two sub-basins to simulate the daily streamflow at the Shigu station. The model parameters are calibrated for the period of 1981–2015 and validated for the period of 2016–2019. The particle swarm optimization (PSO) approach is employed to optimize the parameters of the XAJ model, with the NSE as the objective function.

As input features, the LSTM model takes a time sequence of daily precipitation $\mathbf{p}_i = \mathbf{p}_i[1], \mathbf{p}_i[2], \dots, \mathbf{p}_i[N]$, daily temperature $\mathbf{t}_i = \mathbf{t}_i[1], \mathbf{t}_i[2], \dots, \mathbf{t}_i[N]$ ($i = 1, 2$) of two sub-basins, and XAJ-simulated daily streamflow $\mathbf{q} = \mathbf{q}[1], \mathbf{q}[2], \dots, \mathbf{q}[N]$ over N time steps. Each element of \mathbf{p}_i , \mathbf{t}_i , and \mathbf{q}_i , namely $\mathbf{p}_i[n]$, $\mathbf{t}_i[n]$, and $\mathbf{q}_i[n]$, is a vector of input features for the past n_{seq} days and corresponds to the predictand $\mathbf{o}[n]$, the daily streamflow of Shigu station for time step n . Here n_{seq} is an optimized hyperparameter representing the size of input features. In snow-affected regions such as the SR, it is typically set to a larger value to account for the snow accumulation and melting processes, which can span hundreds of days. In our study, LSTM can also be considered a post-processing model of the XAJ model, similar to the CNN model as a post-processing model of the ECMWF forecast model. The LSTM model is trained by the Adam optimizer and is cross-validated 5-fold using the Randomized Search approach for the period of 1981–2015 (see the Table S2 in the Supplement for details of model hyperparameters). The trained model is then tested for the period of 2016–2019.

3.5 Evaluation metrics

The precipitation forecasts are evaluated using the root mean squared error (RMSE) and relative error (RE) for the ensemble mean and using the CRPS for the total 10 ensemble members. Specifically, we classify the 5 d daily precipitation less than and greater than the 90th percentile of all historic 5 d precipitation during 2002–2019 as light rain events and heavy rain events. The RMSEs are calculated for all rain events and heavy rain events to evaluate the forecasts in predicting common and extreme events, which are both critical for sub-seasonal forecasts that need to inform agricultural planning and flood risk management.

The streamflow forecasts are evaluated using the RMSE, RE, and NSE for general trends and the relative error of the maximum daily flow (REF) for extreme events.

4 Results

4.1 Calibration and validation of the hybrid hydrologic model

The conceptual XAJ model is calibrated for the period of 1981–2015 and validated for the period of 2016–2019. Results in Fig. 3 indicate a satisfactory performance for the standalone XAJ model. The daily NSE values of simulated streamflow are 0.88 and 0.83 during the calibration and validation period. The relative error of streamflow is 1.0 % and 2.6 % during the calibration and validation period. The mean absolute error and relative error of simulated maximum daily flow are $844 \text{ m}^3 \text{ s}^{-1}$ and 17.0 % during the calibration period and $379 \text{ m}^3 \text{ s}^{-1}$ and 7.9 % during the validation period, respectively.

The hybrid hydrologic model is calibrated for the period of 1981–2015 (corresponding to the calibration period of XAJ model and the training and cross-validation period of the LSTM model) and validated for the period of 2016–2019 (corresponding to the validation period of XAJ model and the testing period of the LSTM model). Figure 3 depicts the simulated daily streamflow at Shigu during the validation period, as compared with observations. The results indicate that the daily NSE stands at 0.96 and 0.93 during the calibration and validation period, and the relative error stands at 1.7 % and 2.8 %, respectively. The mean absolute error and relative error of simulated maximum daily flow are $329 \text{ m}^3 \text{ s}^{-1}$ and 7.5 % during the validation period, respectively, indicating the model also has a satisfactory ability to simulate large flood events of the basin. By comparing the simulation accuracy of the standalone XAJ model with that of the hybrid model, it is found that the hybrid model can take advantage of the XAJ outputs and improve the streamflow simulations at Shigu station.

4.2 Evaluation of sub-seasonal precipitation forecasts

The RMSE and RE of areal-averaged EC, EC-QM, and EC-CNN precipitation at different lead time ranges for the period from 2016 to 2019 are provided in Fig. 4, with the error bars representing the 25th–75th percentile interval.

Generally, the EC raw precipitation forecast skills decrease gradually with the increasing lead times and tend to be constant at a relatively low level for lead times of 15–30 d, which is also observed by Lyu et al. (2023) across South-east China. The RMSE averaged over all lead times for the areal-averaged EC forecasts is 1.13 mm d^{-1} . The EC-QM effectively reduces RMSE at all lead times by an average of 0.12 mm d^{-1} ($\sim 11\%$), indicating the effectiveness of QM in improving precipitation at sub-seasonal scales. In contrast, the EC-CNN exhibits $\sim 26\%$ less RMSE compared to EC-QM for all lead times, which reduces the RMSE of EC forecasts by 0.38 mm d^{-1} ($\sim 34\%$). The RE shows a similar trend to RMSE, and the RE of EC, EC-QM, and EC-CNN is

27 %, 36 %, and 42 % averaged over all lead times, respectively.

In particular, the forecast accuracy is improved by EC-CNN forecasts to a relatively steady extent at all lead times, as the RMSE is reduced by 33 %–34 % for different lead time ranges. On the other hand, the RMSE improvements of EC-QM forecasts decrease rapidly with the increase in lead times. For example, the EC-QM reduces the RMSE of EC forecasts by 24 % for the first 10 d, by 11 % for the middle 10 d, and by 4 % for the last 10 d. In addition, EC-CNN forecasts exhibit narrower 25th–75th percentile intervals of RMSE and RE across different initialized dates than raw EC forecasts and EC-QM forecasts, suggesting that the CNN model tends to produce precipitation forecasts with more stable skill metrics across different initialized dates. These results preliminarily demonstrate the superiority of proposed CNN method to the raw EC forecasts and the EC-QM forecasts.

The right-hand panels in Fig. 4 display the variations of RMSE for heavy rain events averaged over SR at lead times of 1–30 d, with the error bars representing the 25th–75th percentile interval. Generally, the RMSE of EC forecasts increases with the increasing lead times for both light and heavy rains. In terms of the heavy rain events, EC-QM shows no improvements as compared to the EC forecasts averaged over all lead times, with the RMSE increasing by $\sim 5\%$, suggesting that QM has a limited ability to improve the forecast skills for extreme precipitation events in the SR. The EC-CNN generally shows slight improvements ($\sim 6\%$) in RMSE as compared to raw forecasts, and the RMSE of EC-CNN forecasts is smaller than that of EC-QM for all lead times, suggesting CNN exhibits advantages over QM for extreme events. This is particularly the case for lead times of 1–10 d, where the RMSE of EC-CNN (EC-QM) forecasts is 26 % (14 %) lower than that of EC forecasts. Overall, these results imply that, for heavy rainfall events, the EC-CNN forecast has an advantage over the EC-QM forecast and also shows a slightly better accuracy than the raw EC forecasts. The RE shows a similar trend to RMSE, as the RE of EC, EC-QM, and EC-CNN is 22 %, 25 %, and 24 % averaged over all lead times. The EC-CNN effectively reduces the bias of heavy rain events at all lead times except for the 16–20 d range.

To investigate the spatial characteristics of precipitation forecasts, Fig. 5 presents the spatial distribution on the RMSE of EC and EC-CNN forecast for lead times of 1–10, 11–20, and 21–30 d. It is clear that the EC-CNN improves the forecast skill of the raw ECMWF forecasts over the majority of the SR for all lead times. For example, the RMSE is reduced from 3–5 mm d^{-1} for EC forecasts to 1–2 mm d^{-1} for EC-CNN forecasts at the northern sub-basin for all lead times. Similar improvements can also be seen around the southern part of the basin; for example the southernmost part of SR sees a RMSE over 10 mm d^{-1} for EC forecasts at lead times of 11–30 d, but this reduces to 6–7 mm d^{-1} for EC-

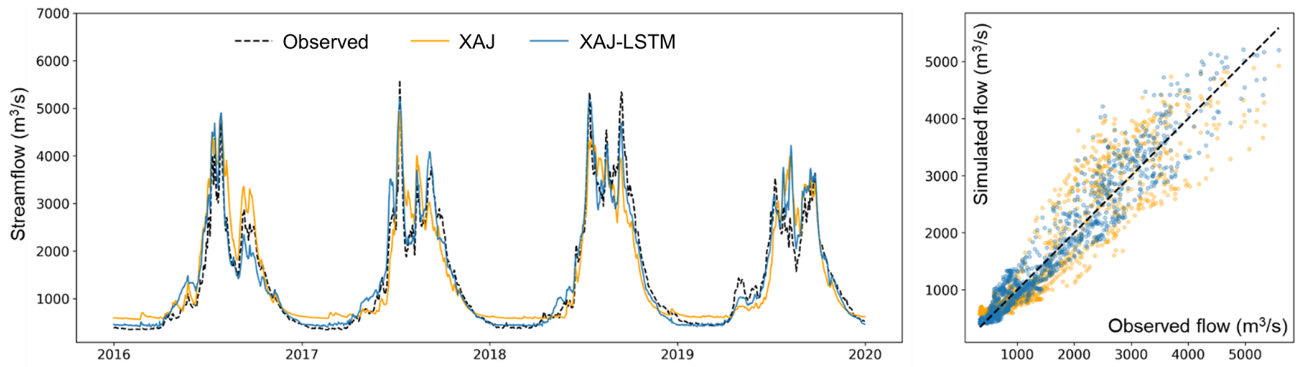


Figure 3. Streamflow validation of the XAJ model and the XAJ-LSTM hydrologic model.

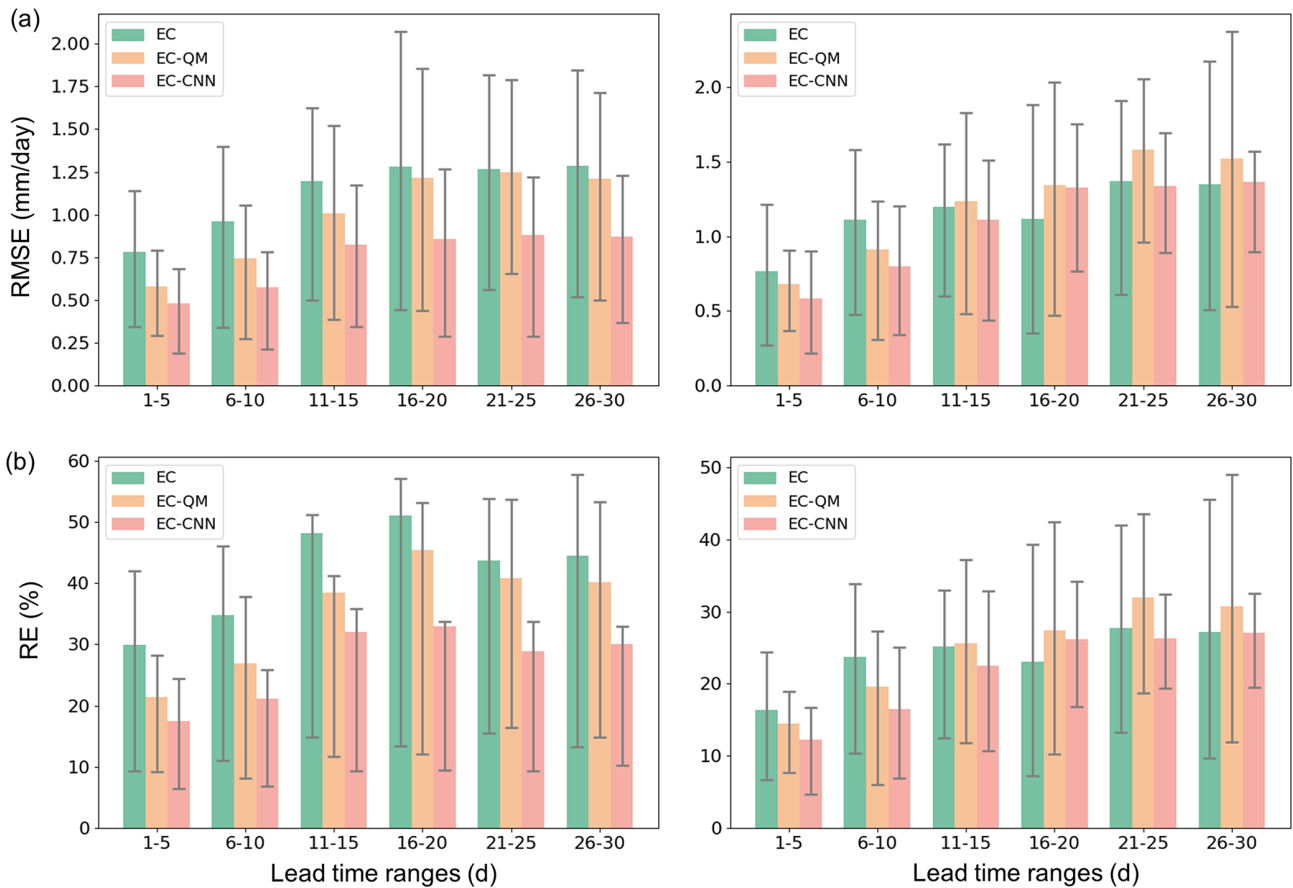


Figure 4. (a) RMSE and (b) RE of all rain events (left) and heavy rain events (right) for the ensemble means of EC, EC-QM, and EC-CNN 5 d precipitation forecasts at lead times of 1–5, 6–10, 11–15, 16–20, 21–25, and 26–30 d. Error bar represents the 25th–75th percentile interval.

CNN forecasts. In addition, by comparing Fig. 5b and c it can be seen that the EC-CNN shows larger improvements than EC-QM across the SR for all lead times. The above results indicate that EC-CNN not only improves the raw forecasts temporally, but also enhances their spatial accuracy across various regions of the SR. This basin-wise improvement allows for more reliable predictions across diverse hydrologi-

cal zones within the SR, which could further benefit the hydrologic modelling.

Figure 6 presents cumulative distribution functions (CDFs) of EC-, EC-QM- and EC-CNN-forecasted precipitation averaged over the SR across all lead times. Notably, the EC-QM forecast consistently aligns well with the observed CDF across all lead times, which reflects the designed purpose of QM to match the empirical distribution through

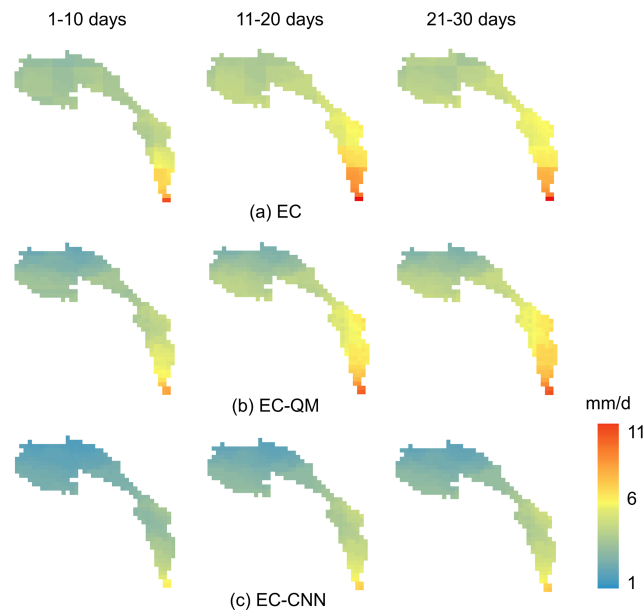


Figure 5. The spatial distribution of RMSE for the ensemble means of (a) EC forecasts, (b) EC-QM, and (c) EC-CNN forecasts averaged over lead times of 1–10, 11–20, and 21–30 d during the test period.

quantile mapping. This result demonstrates EC-QM is good at correcting the raw EC forecast to follow the observed distribution closely, despite an overall large RMSE and RE compared to EC-CNN.

The EC-CNN forecast shows improvement over the EC forecasts and EC-QM forecasts by better approximating the observed CDF for the first 15 d. However, as compared to EC and EC-QM, the EC-CNN begins to deviate more significantly from the observed CDF as lead times increase. Specifically, the EC-CNN forecast appears to concentrate around medium precipitation values for 16–30 d, which underestimates the frequency of both lighter and heavier precipitation events. This pattern suggests that while EC-CNN improves the overall accuracy of light and heavy rains of the raw EC forecasts at all lead times (Fig. 4), the distributional accuracy, particularly for extreme precipitation events, may be compromised over extended lead times. A discussion on the possible cause of biases in CDF for different forecasts is provided in Sect. 5.4.

Figure 7 presents the CRPS of EC-, EC-QM-, and EC-CNN-forecasted precipitation averaged over the SR across the lead times. The CRPS evaluates how close the ensemble forecast distribution is to the observed value, and a value close to zero means a better ensemble forecast. As can be seen in the figure, the CRPS for EC is around 1.1 mm d^{-1} at lead times of 1–10 d, and this increases to around 1.4 mm d^{-1} at lead times of 11–30 d. The EC-QM reduces the CRPS by an average of around 0.1 mm d at all lead times, indicating an improvement in the probabilistic calibration and

sharpness of the ensemble forecasts. The EC-CNN further reduces the CRPS for most of the lead times as compared to the EC-QM, especially for the first 5 d where the CRPS is 0.4 mm d^{-1} lower than EC forecasts and 0.2 mm d^{-1} lower than EC-QM forecasts. This shows that the EC-CNN has an enhanced capability of representing the range of possible outcomes and improving the overall reliability in probabilistic forecasting. Such an advantage also offers better decision-making insights under uncertainty, which is favourable for risk management and planning across various time horizons.

4.3 Evaluation of sub-seasonal streamflow forecasts

Figure 8 shows the RE, REF, RMSE, and NSE of the XAJ-LSTM and XAJ streamflow forecasts driven by EC, EC-QM, and EC-CNN precipitation forecasts, respectively. Results indicate that, for the XAJ-LSTM hybrid model, the accuracy metrics of streamflow forecasts decrease as the lead times increase for all precipitation forecasts. For example, the RE (REF) of streamflow forecasts driven by EC precipitation increases from around 11.6 % (14 %) for 1–10 d to 24 % (23 %) and 28 % (27 %) for 11–20 and 21–30 d, respectively. The EC-QM (EC-CNN) forecasts reduce the RE of the EC forecasts by approximately 6.9 % (16.4 %), 13.8 % (32.5 %), and 12.5 % (26.8 %), respectively, and reduce the REF of the EC forecasts by approximately 14.3 % (28.6 %), 10.4 % (35.7 %), and 13.3 % (25.6 %), respectively. It is noted that the improvements brought by EC-QM and EC-CNN are larger in lead times of 11–20 d than in 1–10 d, which was also observed by Zhang et al. (2023), Lyu et al. (2023), and Li et al. (2024b) in specific cases.

For the standalone XAJ model, the RE (REF) of streamflow forecasts driven by EC raw forecasts increases from around 18 % (21 %) for 1–10 d to 31 % (33 %) and 34 % (31 %) for 11–20 and 21–30 d, respectively. The EC-QM (EC-CNN) forecasts reduce the RE of the EC forecasts by approximately 5.6 % (9.4 %), 8.1 % (18.4 %), and 0.6 % (12.4 %) for the 1–10, 11–20, and 21–30 d lead times, respectively. For the relative error of maximum daily flow, the EC-QM (EC-CNN) forecasts reduce it by approximately 9.4 % (26.7 %), 11.6 % (24.8 %), and 0.9 % (5.8 %) for each corresponding lead time range.

The above results indicate (1) that the streamflow and flood biases are smaller for XAJ-LSTM than for XAJ for all lead times and (2) that improvements in EC-CNN and EC-QM precipitation forecast enhance the streamflow forecast accuracy more effectively for the XAJ-LSTM model than for the XAJ model. Notably, the EC-CNN (EC-QM)-driven XAJ-LSTM streamflow forecast sees 20%–31% (6%–12%) less RMSE than that driven by EC forecasts over different lead time periods. On the other hand, the EC-CNN (EC-QM)-driven XAJ streamflow forecasts only see 7%–11% (1%–7%) less RMSE compared to that driven by EC, reflecting a much less improvement compared to those driven by XAJ-LSTM. A similar trend can also be observed for

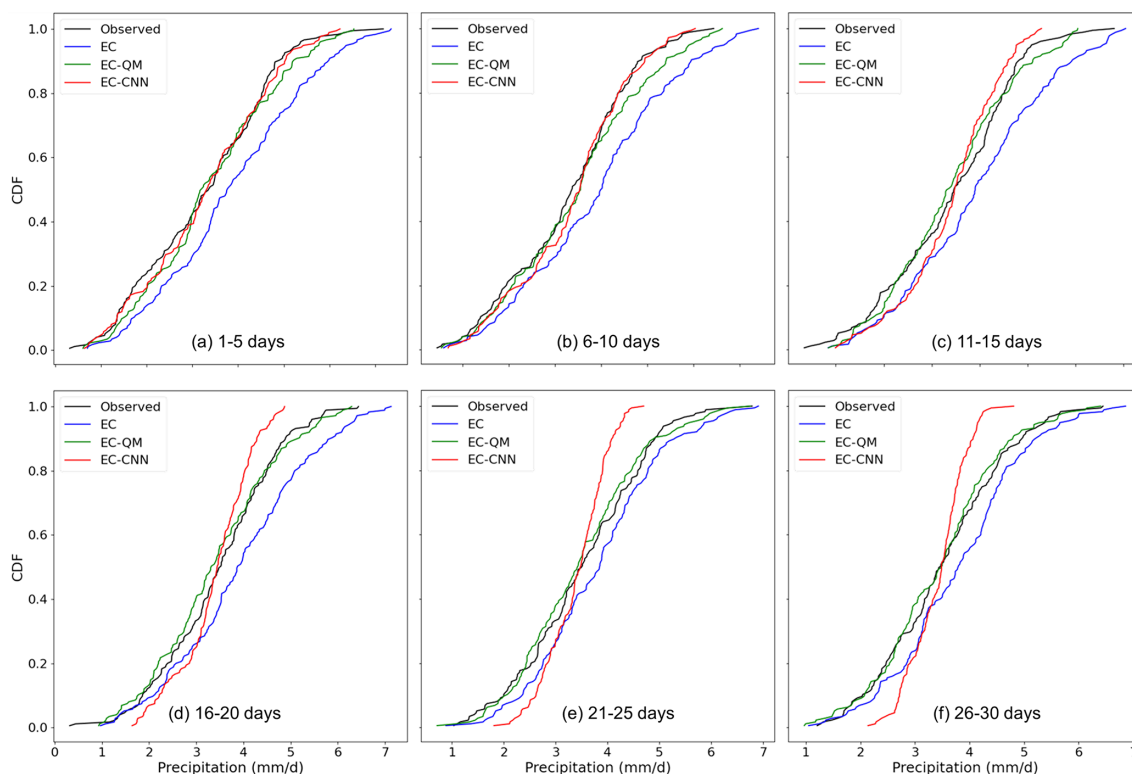


Figure 6. The cumulative distribution function (CDF) of areal-averaged precipitation for observed precipitation and the ensemble means of EC, EC-QM, and EC-CNN forecasts at different lead times during the test period.

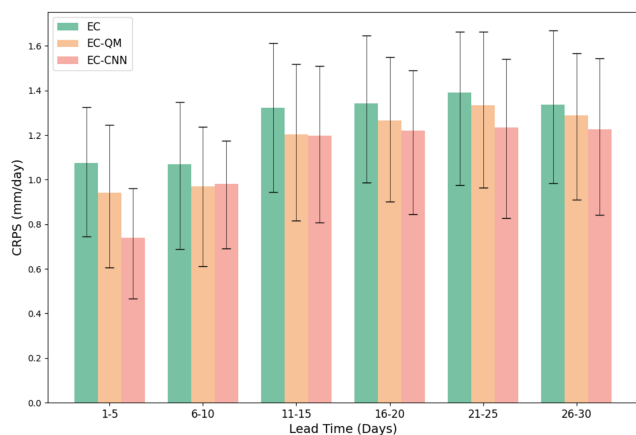


Figure 7. The CRPS of areal-averaged precipitation for the EC, EC-QM, and EC-CNN ensemble forecasts at different lead times during the test period. Error bar represents the 25th–75th percentile interval.

NSE, as XAJ-LSTM shows more improvement than XAJ when EC precipitation forecasts are replaced by EC-CNN and EC-QM precipitation forecasts. This result suggests that improving sub-seasonal precipitation forecasts may not necessarily translate to a streamflow improvement because it is

not only related to the skill of precipitation forecasts but also, to a large extent, the hydrologic model.

It is also noted that, despite the NSE values improving with the EC-CNN precipitation forecasts, they are mostly negative for both hydrologic models. This suggests further improvements may be required to achieve a more accurate hydrologic forecast at sub-seasonal scales. A discussion on this aspect is provided in Sect. 5.4.

Figure 9 presents examples of XAJ-LSTM streamflow ensemble forecasts initialized on different dates, with the RE of total forecast flow presented in each subplot. In most cases, the EC-CNN forecasts can reduce the streamflow bias in a more flexible manner than the EC-QM forecasts, resulting in more accurate overall streamflow predictions across different dates. For example, the CNN model decreases (increases) the EC precipitation and hence the forecast streamflow issued on 6 June 2017 (8 August 2019), which improves the forecast skills in both cases. The EC-CNN reduces the relative error from 22.1 % of raw EC forecasts to -2.5 % for the 30 d streamflow forecast issued on 6 June 2017 and reduces the relative error from -21.5 % of raw EC forecasts to -9.2 % for the 30 d streamflow forecast issued on 8 August 2019. On the other hand, the QM reduces the precipitation and hence the streamflow forecasts for both dates, which reduces the relative error to 11.0 % on June 2017 but increases the relative error to -27.3 % on August 2019. Similarly, for the fore-

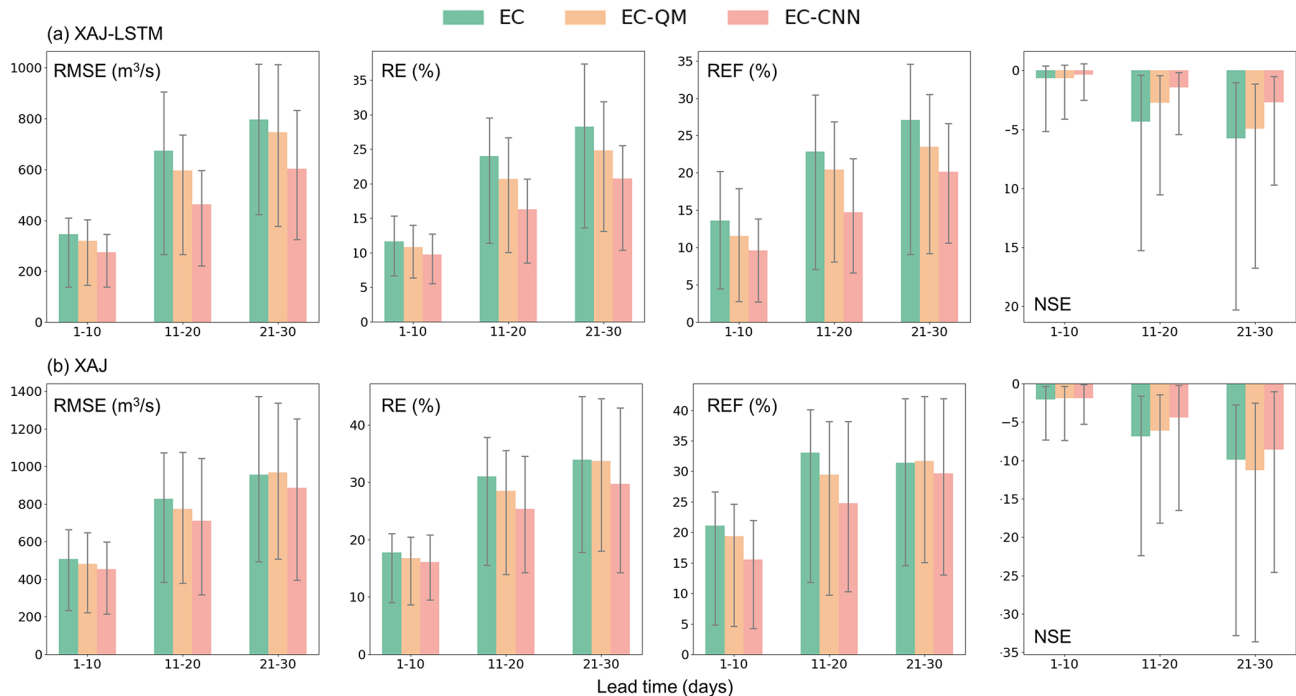


Figure 8. The RMSE, RE, REF, and NSE for the (a) XAJ-LSTM and (b) XAJ streamflow forecasts driven by the ensemble means of EC, EC-QM, and EC-CNN forecasts for lead times of 1–10, 11–20, and 21–30 d. Error bar represents the 25th–75th percentile interval.

cast issued on 11 August 2017, EC-CNN decreases the EC precipitation for lead times of 1–20 d and increases it for lead times of 21–30 d, which alleviates the streamflow overestimation in late August and underestimation in early September. However, EC-QM consistently predicts lower precipitation and hence streamflow compared to EC forecasts at all lead times, worsening the underestimation in early September.

Figure 10 presents the CRPS of EC-, EC-QM-, and EC-CNN-driven XAJ-LSTM streamflow forecasts at Shigu across the lead times. The CRPS for EC is around $120 \text{ m}^3 \text{ s}^{-1}$ at lead times of 1–5 d and increases rapidly to around $300 \text{ m}^3 \text{ s}^{-1}$ at lead times of 6–10 d and further to $500 \text{ m}^3 \text{ s}^{-1}$ at lead times of 21–30 d. The EC-QM reduces the CRPS by an average of around $65 \text{ m}^3 \text{ s}^{-1}$ at all lead times, and the EC-CNN further reduces the CRPS for most of the lead times as compared to the EC-QM, especially for the lead times of 6–20 d, where the CRPS is about $60 \text{ m}^3 \text{ s}^{-1}$ lower than EC forecasts and $25 \text{ m}^3 \text{ s}^{-1}$ lower than EC-QM forecasts. However, for lead times of 26–30 d, the CRPS of EC-CNN is slightly larger than that EC-QM, indicating the advantage of EC-CNN in ensemble forecasting is not evident for extended forecast lead times. Nevertheless, the EC-CNN improves the overall reliability in probabilistic streamflow forecasting for all lead times as compared to EC and for most lead times as compared to EC-QM, which can benefit the downstream water resources management under uncertainty.

5 Discussion

5.1 Deep learning models can outperform traditional statistical downscaling methods in both mean and extremes

Traditional post-processing methods for precipitation forecasts often rely on local precipitation forecasts as the sole predictor, which can limit their ability to fully utilize the spatial information embedded in raw forecasts (Sun and Lan, 2021). In this study, an ensemble of enhanced CNN post-processing models with ResNet blocks and a weighted loss function specialized on extreme events is established to investigate its potential to overcome these limitations by establishing multi-dimensional relationships between atmospheric circulation predictors and local precipitation.

We compare the CNN model with the commonly used quantile mapping (QM) bias correction method. It is noted that, for several lead time ranges, EC-QM forecasts show no improvements in RMSEs compared to those of raw EC forecasts. This was also observed by some of the recent studies using QM for statistical downscaling precipitation. For example, Li et al. (2023), Huang et al. (2022), and Mao et al. (2015) show that while QM is generally effective in adjusting model bias towards observations, it does not always lead to improvements of the forecast accuracy. One plausible reason could be the limited applicability of the relatively simple QM method. Specifically, QM primarily adjusts the distribution of forecasted values towards the distribution of his-

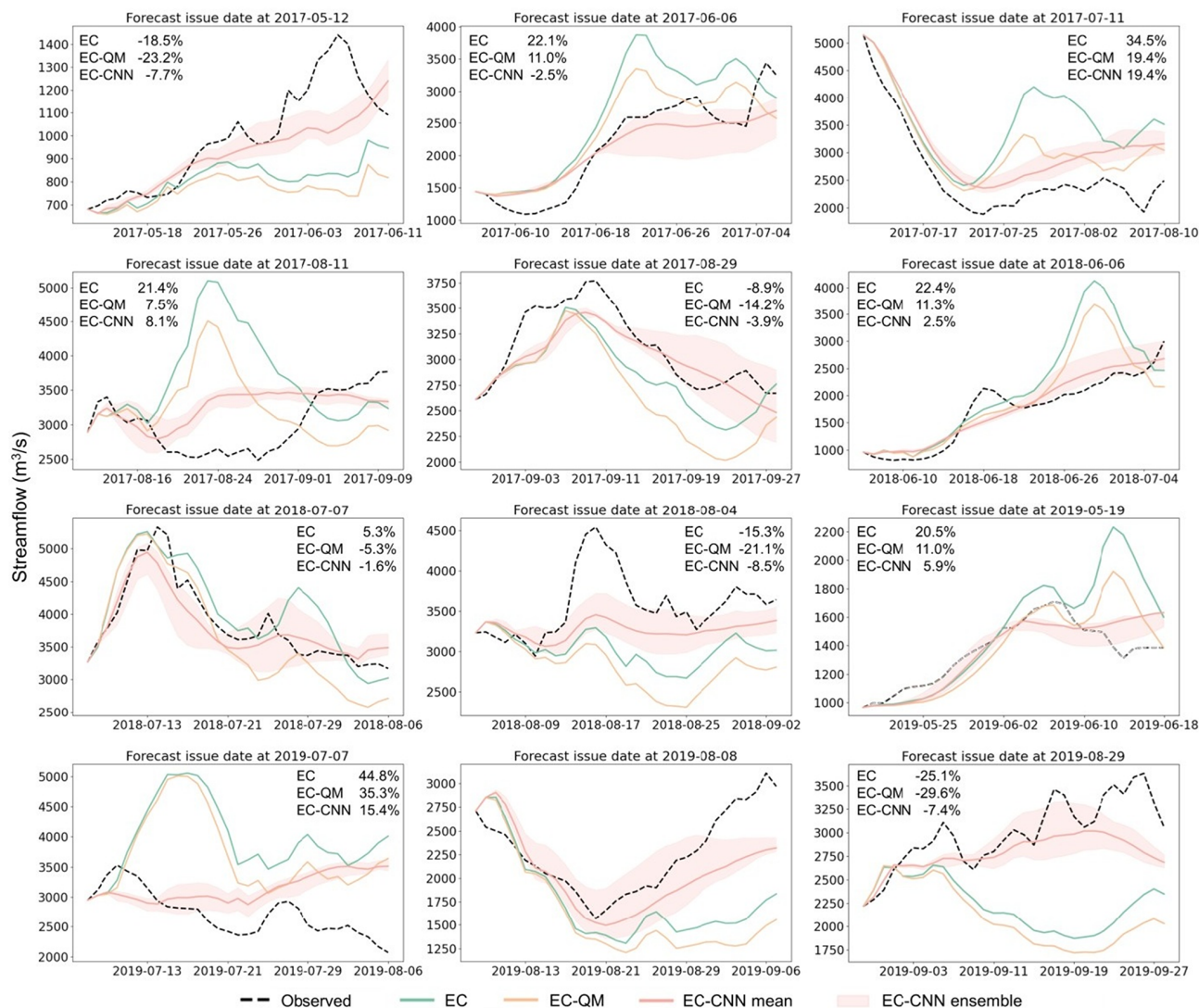


Figure 9. Examples of sub-seasonal XAJ-LSTM streamflow forecasts for a lead time of 30 d driven by EC, EC-QM, and ensemble EC-CNN precipitation forecasts. Shaded areas represent the 25th–75th percentile. The relative error of total forecast flow is shown in each subplot.

torical observations, with no account of the atmospheric conditions associated with those forecasts. However, physics-based numerical weather predictions involve complex and nonlinear errors that QM may not be able to fully correct.

On the other hand, the CNN model improves the RMSE and RE of forecast precipitation at all lead times and outperforms QM in terms of capturing the general trends, predicting extreme precipitation events, and approximating the probabilistic distribution at sub-seasonal scales. This superior performance is likely due to the specialized loss function that balances the prediction of light rain events and extreme events by incorporating the mean squared error and the threat score. This balance is crucial for sub-seasonal forecasts, where both event types impact water resource management. In general, the CNN structure used in our study is not only effective and easy to implement but also more compu-

tationally efficient than more complex CNN variations like SmaAt-UNet. Nevertheless, newer variants may better leverage multi-scale spatial information and incorporate multiple auxiliary predictors relevant to local weather conditions (Rasp and Lerch, 2018; Peng et al., 2020; Baño-Medina et al., 2020). Future research will focus on integrating these variants with new loss functions to achieve more desirable forecast outcomes.

The rapid development of AI-based weather prediction models in recent years, such as Pangu and GraphCast, has also demonstrated the potential of these models to achieve forecast skills comparable to state-of-the-art physics-based models (Bi et al., 2023; Lam et al., 2023). In comparison, our CNN-based statistically downscaled model of ECMWF precipitation forecasts offers improved sub-seasonal forecast skills with significantly lower computational resources,

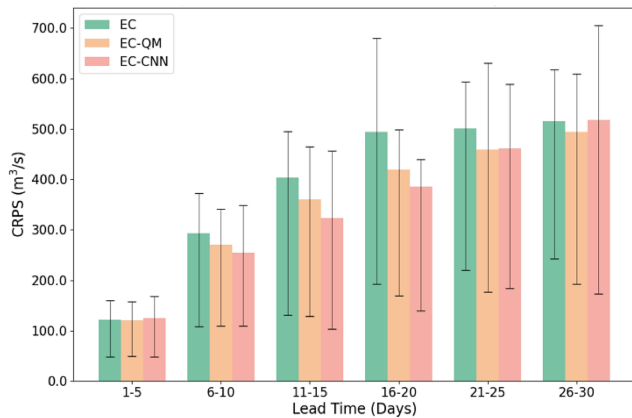


Figure 10. The CRPS of streamflow forecasts driven by the EC, EC-QM, and EC-CNN ensemble forecasts at different lead times during the test period. Error bar represents the 25th–75th percentile interval.

which could make it a practical and efficient tool for operational use in local meteorological or water agencies to provide high-quality forecasts and issue early warnings. Our results also underscore the potential of combining advanced AI techniques with physics-based forecasting methods to achieve superior performance and operational efficiency in weather prediction.

5.2 Better sub-seasonal precipitation forecasts may not guarantee better streamflow forecasts

The evaluation of sub-seasonal streamflow forecasts in Sect. 4.3 reveals a complex relationship between precipitation forecast accuracy and streamflow forecast performance. For example, the results presented in Fig. 8 demonstrate that while improvements in precipitation forecasts generally lead to better streamflow forecasts, this relationship is not straightforward and can be influenced significantly by the choice of hydrologic model.

For example, a notable finding is that the hybrid XAJ-LSTM model shows much more substantial streamflow improvements with better precipitation forecasts compared to the standalone XAJ model. Specifically, the XAJ-LSTM model, which combines the strengths of LSTM networks and the XAJ hydrologic model, benefits significantly from the enhanced accuracy of EC-CNN forecasts. This model demonstrates a considerable reduction in RMSE for streamflow predictions over various lead times. On the other hand, the standalone XAJ model exhibits marginal improvements when driven by the same enhanced precipitation forecasts.

This disparity suggests that while advanced precipitation forecasts provide more accurate inputs, the ability of hydrologic models to effectively utilize these inputs is crucial. Similar findings are also reported by Valdez et al. (2022), for lead times of 7 d, who attribute the potential degradation of streamflow forecasts to other sources of uncertainties

that may cancel out the added values of precipitation forecast improvements. The integration of machine learning (LSTM) and physical process representations (XAJ) allows it to better capture the long-term dependencies in hydrological processes, making it more responsive to the quality of precipitation forecasts at sub-seasonal scales. This synergy between the two models enables to leverage the strengths of both conceptual understanding and data-driven prediction, which can also be extended to other basins with similar hydrological characteristics for addressing the sub-seasonal forecasting challenges.

5.3 Attribution of the XAJ-LSTM streamflow forecast error

To identify the possible sources of error for the XAJ-LSTM streamflow forecasts, an error decomposition method is employed to break down the total forecast error into its constituent parts. The specific contributions of each error source are isolated by calculating the RMSE of the ensemble mean streamflow forecast driven by observed precipitation and temperature (i.e. the hydrologic modelling error, E_m), the RMSE of the ensemble mean streamflow forecasts driven by forecast precipitation and observed temperature (i.e. the precipitation forecast error, E_p), and the RMSE of the ensemble mean streamflow forecasts driven by observed precipitation and forecast temperature (i.e. the temperature forecast error, E_t). Note that the total error between the observed streamflow and the forecast streamflow driven by forecast precipitation and temperature may not be equal to the sum of E_m , E_p , and E_t , due to the interacting effects between multiple sources of error. This is manifested by the analysis result that the individual contributions of E_p , E_m , and E_t to the total error add up to a value greater than 100 %, indicating that there is a compensatory effect between multiple sources of error that reduces the total error.

Figure 11 depicts the individual contribution of E_p , E_m , and E_t to their combined error. In general, the hydrologic modelling error E_m dominates for lead times of 1–3 d, accounting for over 50 % of the three sources of error combined. The ratio of E_m decreases rapidly with the increase in lead times and reaches a steady value of around 0.3 after the lead time of 15 d. The contribution ratio of precipitation forecast error E_p rises rapidly for lead times of 1–7 d and stands at a steady value of around 0.6 after the lead time of 15 d. The temperature forecast error E_t , while present, has a less pronounced impact compared to E_m and E_p , accounting for 5 %–10 % of the combined error. This is an expected result as precipitation generally impacts the streamflow more significantly than temperature.

5.4 Limitations of this study

One limitation of the proposed EC-CNN model is its reduced accuracy in capturing the CDF over lead times extending be-

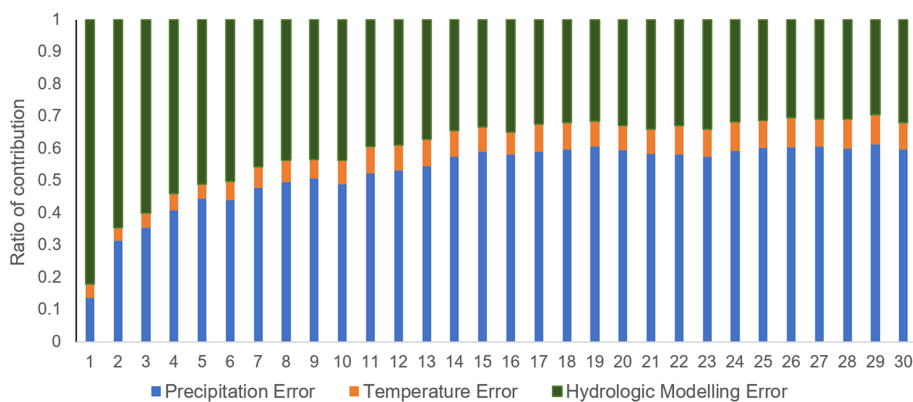


Figure 11. Contribution of precipitation forecast errors, temperature forecast errors, and hydrologic modelling errors to their combined error.

yond 15 d. While EC-CNN outperforms in terms of RMSE and RE for both light and heavy rainfall events (Fig. 4), its CDF deviates from observed patterns for these longer lead times. In contrast, EC and EC-QM tend to align more closely with observed CDFs at these lead times. We attribute this to the following possible reason.

Over extended lead times (> 15 d), extreme precipitation values of EC and EC-QM forecasts tend to be more incorrectly assigned to specific times, leading to, for instance, storm-level precipitation predictions on dry days or nearly zero precipitation predictions on storm days. While these misplaced extremes inflate daily errors, they still allow the overall CDF of the forecast to retain both high and low ends of the precipitation distribution. The EC-CNN model, however, is designed to minimize daily errors by adjusting outliers and bringing exaggerated values closer to moderate levels, thereby reducing large forecast errors. For example, when EC forecasts a high precipitation event on a dry day, EC-CNN mitigates this by lowering the extreme to a more typical value. While this adjustment helps decrease RMSE and RE, it compresses the distribution toward the centre by reducing the frequency of both extreme high and low precipitation values. This approach limits the model ability to capture the full distribution, resulting in a CDF that is overly concentrated around moderate values.

Another limitation is the relatively low Nash–Sutcliffe efficiency (NSE) values in streamflow forecasts, especially over extended lead times. Despite improvements in streamflow forecast accuracy due to EC-CNN and the XAJ-LSTM, NSE values are found predominantly negative. This can be primarily due to the inaccuracies in the precipitation forecasts that drive these hydrologic models, as high NSE values require precipitation inputs to be accurate both spatially and temporally. Improving the hydrologic model alone is unlikely to address this issue substantially, as it depends heavily on input accuracy (Sect. 5.3).

Nevertheless, with our proposed coupled EC-CNN and XAJ-LSTM framework, the overall relative error of forecast flow can be reduced to $\sim 10\%$ for the next 10 d and $\sim 20\%$

for the next 30 d (Fig. 7), which can have implications for water management and disaster prevention. Future improvements in NSE could focus on refining precipitation forecasting with more advanced AI models. Additionally, LSTM model training on multiple basins and fine-tuning on specific target basins could further enhance the streamflow accuracy over extended lead times (Kratzert et al., 2019).

6 Summary and conclusions

This study proposes a deep-learning-based modelling framework for sub-seasonal hydrometeorological forecasts (i.e. precipitation and streamflow) for a lead time of up to 30 d. The framework couples (1) an ensemble of enhanced CNN models with ResNet blocks for statistically downscaling ECMWF raw precipitation ensemble forecasts to (2) a hybrid hydrologic model integrating the conceptual XAJ model and LSTM for streamflow forecasting. The CNN models incorporate a specialized loss function that combines the continuous form of TS and MAE.

By applying the modelling framework to the source region of the Yangtze River Basin, we show that the CNN-based downscaling model exhibits advantages over quantile mapping in improving the precipitation forecasts in terms of the general trends, extreme events, and ensemble distribution. The CNN-based model consistently outperforms the raw ECMWF forecasts and the traditional QM approach across all lead times, achieving an average RMSE value around 30 % lower than both forecasts. This improvement is also noted in extreme precipitation events, as demonstrated by approximately 6 % and 10 % lower RMSE of the CNN for heavy rain events as compared to raw forecasts and QM forecasts.

With these precipitation forecasts serving as meteorological drivers of a hybrid XAJ-LSTM hydrologic model, it is found that CNN-based models can reduce the relative error of streamflow forecasts by 16 %–33 % compared to raw precipitation forecasts, particularly for longer lead times.

This outperforms QM, which reduces the relative error of streamflow by 7%–14% compared to raw precipitation forecasts. The CNN-based precipitation forecasts also prove effective in deriving more reliable streamflow forecasts during extreme hydrological events (such as floods) for the XAJ-LSTM model, with the average relative error of maximum daily flow reduced by 26%–36%. However, for the standalone XAJ model, the streamflow forecasts show marginal improvements with the same CNN enhanced precipitation forecasts. This highlights the importance of understanding the effectiveness of the hydrologic model as part of the sub-seasonal hydrometeorological modelling chain.

From a practical perspective, the proposed modelling framework is computationally efficient, requiring lower computational resources compared to fully AI models, traditional dynamic downscaling methods, and distributed hydrologic models. This makes it a viable tool for operational use in local meteorological and water management agencies to provide more accurate forecasts and issue early warnings. This study also shows the potential of combining advanced AI techniques with traditional hydrologic modelling approaches to achieve superior performance in sub-seasonal hydrometeorological forecasting, offering a robust and adaptable solution for effective water resources management and disaster preparedness.

Code availability. The CNN model for statistically downscaling and bias-correcting the ECMWF raw forecasts is deposited in a Zenodo repository (<https://doi.org/10.5281/zenodo.12664798>; Dong et al., 2024a). The LSTM and the hybrid hydrologic model are developed and configured using the NeuralHydrology package, available at <https://neuralhydrology.readthedocs.io/en/latest/index.html> (Kratzert et al., 2022).

Data availability. The ECMWF forecast data and observed precipitation and temperature data are all deposited in a Zenodo repository (<https://doi.org/10.5281/zenodo.12664851>; Dong et al., 2024b).

Supplement. The supplement related to this article is available online at <https://doi.org/10.5194/hess-29-2023-2025-supplement>.

Author contributions. ND contributed to the research design; compiled the dataset; and conducted the data processing, analysis, and manuscript preparation. HH contributed to the research design, data processing, and code development. MY, JW, SX, and HK contributed to the manuscript editing.

Competing interests. The contact author has declared that none of the authors has any competing interests.

Disclaimer. Publisher's note: Copernicus Publications remains neutral with regard to jurisdictional claims made in the text, published maps, institutional affiliations, or any other geographical representation in this paper. While Copernicus Publications makes every effort to include appropriate place names, the final responsibility lies with the authors.

Financial support. This research has been supported by the National Key Research and Development Program of China (grant no. 2023YFC3081000), the National Natural Science Foundation of China (grant no. 42401053), the German Federal Ministry of Science of Education (BMBF) through funding of the KARE_II project (grant no. 01LR2006D1), the China Power Construction Corporation Technology Project (grant no. DJ-HXGG-2021-04), the Key R&D Plan Project in Yunnan Province (grant no. 202203AA080010), and the IWHR Basic Operational Funds (grant nos. SKL2024YJZD02 and WR110145B0032024).

Review statement. This paper was edited by Xing Yuan and reviewed by two anonymous referees.

References

- Abrahart, R. J., Anctil, F., Coulibaly, P., Dawson, C. W., Mount, N. J., See, L. M., Shamseldin, A. Y., Solomatine, D. P., Toth, E., and Wilby, R. L.: Two decades of anarchy? Emerging themes and outstanding challenges for neural network river forecasting, *Prog. Phys. Geogr.*, 36, 480–513, <https://doi.org/10.1177/0309133312444943>, 2012.
- Addor, N., Do, H. X., Alvarez-Garretón, C., Coxon, G., Fowler, K., and Mendoza, P. A.: Large-sample hydrology: recent progress, guidelines for new datasets and grand challenges, *Hydrol. Sci. J.*, 65, 712–725, <https://doi.org/10.1080/02626667.2019.1683182>, 2020.
- Adnan, R. M., Liang, Z., Trajkovic, S., Zounemat-Kermani, M., Li, B., and Kisi, O.: Daily streamflow prediction using optimally pruned extreme learning machine, *J. Hydrol.*, 577, 123981, <https://doi.org/10.1016/j.jhydrol.2019.123981>, 2019.
- Balint, G., Csik, A., Bartha, P., Gauzer, B., and Bonta, I.: Application of meteorological ensembles for Danube flood forecasting and warning, in: *Transboundary Floods: Reducing Risks through Flood Management*, edited by: Marsalek, J., Stancalie, G., and Balint, G., NATO Sci. Ser., Springer, Dordrecht, 57–68, https://doi.org/10.1007/1-4020-4902-1_6, 2006.
- Baño-Medina, J., Manzanar, R., and Gutiérrez, J. M.: Configuration and intercomparison of deep learning neural models for statistical downscaling, *Geosci. Model Dev.*, 13, 2109–2124, <https://doi.org/10.5194/gmd-13-2109-2020>, 2020.
- Baño-Medina, J., Manzanar, R., and Gutiérrez, J. M.: On the suitability of deep convolutional neural networks for continental-wide downscaling of climate change projections, *Clim. Dynam.*, 57, 2941–2951, <https://doi.org/10.1007/s00382-021-05847-0>, 2021.
- Bauer, P., Thorpe, A., and Brunet, G.: The quiet revolution of numerical weather prediction, *Nature*, 525, 47–55, <https://doi.org/10.1038/nature14956>, 2015.

- Bi, K., Xie, L., Zhang, H., Chen, X., Gu, X., and Tian, Q.: Accurate medium-range global weather forecasting with 3D neural networks, *Nature*, 619, 533–538, <https://doi.org/10.1038/s41586-023-06185-3>, 2023.
- Bierkens, M. F. P.: Global hydrology 2015: State, trends, and directions, *Water Resour. Res.*, 51, 4923–4947, <https://doi.org/10.1002/2015WR017173>, 2015.
- Bonavita, M.: On some limitations of current machine learning weather prediction models, *Geophys. Res. Lett.*, 51, e2023GL107377, <https://doi.org/10.1029/2023GL107377>, 2024.
- Bremnes, J. B.: Ensemble postprocessing using quantile function regression based on neural networks and Bernstein polynomials, *Mon. Weather Rev.*, 148, 403–414, <https://doi.org/10.1175/MWR-D-19-0227.1>, 2020.
- Brotzge, J. A., Berchhoff, D., Carlis, D. L., Carr, F. H., Carr, R. H., Gerth, J. J., Gross, B. D., Hamill, T. M., Haupt, S. E., Jacobs, N., McGovern, A., Stensrud, D. J., Szatkowski, G., Szunyogh, I., and Wang, X.: Challenges and opportunities in numerical weather prediction, *B. Am. Meteorol. Soc.*, 104, E698–E705, <https://doi.org/10.1175/BAMS-D-22-0172.1>, 2023.
- Cannon, A. J., Sobie, S. R., and Murdock, T. Q.: Bias correction of GCM precipitation by quantile mapping: How well do methods preserve changes in quantiles and extremes?, *J. Climate*, 28, 6938–6959, <https://doi.org/10.1175/JCLI-D-14-00754.1>, 2015.
- Chen, G. and Wang, W.-C.: Short-term precipitation prediction for contiguous United States using deep learning, *Geophys. Res. Lett.*, 49, e2022GL097904, <https://doi.org/10.1029/2022GL097904>, 2022.
- Cho, D., Yoo, C., Im, J., and Cha, D. H.: Comparative assessment of various machine learning-based bias correction methods for numerical weather prediction model forecasts of extreme air temperatures in urban areas, *Earth Space Sci.*, 7, e2019EA000740, <https://doi.org/10.1029/2019EA000740>, 2020.
- Cloke, H. L. and Pappenberger, F.: Ensemble flood forecasting: A review, *J. Hydrol.*, 375, 613–626, <https://doi.org/10.1016/j.jhydrol.2009.06.005>, 2009.
- Crochemore, L., Ramos, M.-H., and Pappenberger, F.: Bias correcting precipitation forecasts to improve the skill of seasonal streamflow forecasts, *Hydrol. Earth Syst. Sci.*, 20, 3601–3618, <https://doi.org/10.5194/hess-20-3601-2016>, 2016.
- de Andrade, F. M., Young, M. P., MacLeod, D., Hirons, L. C., Woolnough, S. J., and Black, E.: Subseasonal precipitation prediction for Africa: Forecast evaluation and sources of predictability, *Weather Forecast.*, 36, 265–284, <https://doi.org/10.1175/WAF-D-20-0102.1>, 2021.
- Dehshiri, S. S. H. and Firoozabadi, B.: A multi-objective framework to select numerical options in air quality prediction models: A case study on dust storm modeling, *Sci. Total Environ.*, 863, 160681, <https://doi.org/10.1016/j.scitotenv.2022.160681>, 2023.
- Di Luca, A., de Elía, R., and Laprise, R.: Potential for added value in precipitation simulated by high-resolution nested regional climate models and observations, *Clim. Dynam.*, 44, 2519–2537, <https://doi.org/10.1007/s00382-011-1068-3>, 2015.
- Dong, N., Wei, J., Yang, M., Yan, D., Yang, C., Gao, H., Arnault, J., Laux, P., Zhang, X., Liu, Y., and Niu, J.: Model estimates of China’s terrestrial water storage variation due to reservoir operation, *Water Resour. Res.*, 58, e2021WR031787, <https://doi.org/10.1029/2021WR031787>, 2022.
- Dong, N., Yang, M., Wei, J., Arnault, J., Laux, P., Xu, S., Wang, H., Yu, Z., and Kunstmann, H.: Toward improved parameterizations of reservoir operation in ungauged basins: A synergistic framework coupling satellite remote sensing, hydrologic modeling, and conceptual operation schemes, *Water Resour. Res.*, 59, e2022WR033026, <https://doi.org/10.1029/2022WR033026>, 2023.
- Dong, N., Hao, H., Yang, M., Wei, J., Xu, S., and Kunstmann, H.: Model, Zenodo [code], <https://doi.org/10.5281/zenodo.12664798>, 2024a.
- Dong, N., Hao, H., Yang, M., Wei, J., Xu, S., and Kunstmann, H.: Data, Zenodo [data set], <https://doi.org/10.5281/zenodo.12664851>, 2024b.
- Ebert-Uphoff, I. and Hilburn, K.: Evaluation, tuning and interpretation of neural networks for working with images in meteorological applications, *B. Am. Meteorol. Soc.*, 101, E1654–E1677, <https://doi.org/10.1175/BAMS-D-19-0324.1>, 2020.
- Ferranti, L., Corti, S., and Janousek, M.: Flow-dependent verification of the ECMWF ensemble over the Euro-Atlantic sector, *Q. J. Roy. Meteor. Soc.*, 144, 317–326, <https://doi.org/10.1002/qj.3204>, 2018.
- Gao, S., Huang, D., Du, N., Ren, C., and Yu, H.: WRF ensemble dynamical downscaling of precipitation over China using different cumulus convective schemes, *Atmos. Res.*, 271, 106116, <https://doi.org/10.1016/j.atmosres.2022.106116>, 2022.
- Gassman, P. W., Reyes, M. R., Green, C. H., and Arnold, J. G.: The Soil and Water Assessment Tool: Historical development, applications, and future research directions, *Trans. ASABE*, 57, 1211–1250, <https://doi.org/10.13031/2013.23637>, 2014.
- Gudmundsson, L., Bremnes, J. B., Haugen, J. E., and Engen-Skaugen, T.: Technical Note: Downscaling RCM precipitation to the station scale using statistical transformations – a comparison of methods, *Hydrol. Earth Syst. Sci.*, 16, 3383–3390, <https://doi.org/10.5194/hess-16-3383-2012>, 2012.
- Ham, Y.-G., Kim, J.-H., and Luo, J.-J.: Deep learning for multi-year ENSO forecasts, *Nature*, 573, 568–572, <https://doi.org/10.1038/s41586-019-1559-7>, 2019.
- Han, L., Chen, M., Chen, K., Chen, H., Zhang, Y., Lu, B., Song, L., and Qin, R.: A deep learning method for bias correction of ECMWF 24–240 h forecasts, *Adv. Atmos. Sci.*, 38, 1444–1459, <https://doi.org/10.1007/s00376-021-0434-2>, 2021.
- Hao, H., Dong, N., Yang, M., Wei, J., Zhang, X., Xu, S., Yan, D., Ren, L., Leng, G., Chen, L., and Zhou, X.: The changing hydrology of an irrigated and dammed Yangtze River: Streamflow, extremes, and lake hydrodynamics, *Water Resour. Res.*, 60, e2024WR037841, <https://doi.org/10.1029/2024WR037841>, 2024.
- Horat, N. and Lerch, S.: Deep Learning for Postprocessing Global Probabilistic Forecasts on Subseasonal Time Scales, *Mon. Weather Rev.*, 152, 667–687, <https://doi.org/10.1175/MWR-D-23-0112.1>, 2024.
- Hu, C. H., Guo, S. L., Xiong, L. H., and Peng, D. Z.: A modified Xin’anjiang model and its application in northern China, *Hydrol. Res.*, 36, 175–192, <https://doi.org/10.2166/nh.2005.0013>, 2005.
- Huang, Z., Zhao, T., Xu, W., Cai, H., Wang, J., Zhang, Y., Liu, Z., Tian, Y., Yan, D., and Chen, X.: A Seven-Parameter Bernoulli-Gamma-Gaussian Model to Calibrate Subseasonal to Seasonal Precipitation Forecasts, *J. Hydrol.*, 610, 127896, <https://doi.org/10.1016/j.jhydrol.2022.127896>, 2022.

- Humphrey, G. B., Gibbs, M. S., Dandy, G. C., and Maier, H. R.: A hybrid approach to monthly streamflow forecasting: Integrating hydrological model outputs into a Bayesian artificial neural network, *J. Hydrol.*, 540, 623–640, <https://doi.org/10.1016/j.jhydrol.2016.06.026>, 2016.
- Jaun, S., Ahrens, B., Walser, A., Ewen, T., and Schär, C.: A probabilistic view on the August 2005 floods in the upper Rhine catchment, *Nat. Hazards Earth Syst. Sci.*, 8, 281–291, <https://doi.org/10.5194/nhess-8-281-2008>, 2008.
- Jiang, M., Weng, B., Chen, J., Huang, T., Ye, F., and You, L.: Transformer-enhanced spatiotemporal neural network for post-processing of precipitation forecasts, *J. Hydrol.*, 630, 130720, <https://doi.org/10.1016/j.jhydrol.2024.130720>, 2024.
- Jiang, Z., Yang, S., Liu, Z., Xu, Y., Xiong, Y., Qi, S., Pang, Q., Xu, J., Liu, F., and Xu, T.: Coupling machine learning and weather forecast to predict farmland flood disaster: A case study in Yangtze River basin, *Environ. Model. Softw.*, 155, 105436, <https://doi.org/10.1016/j.envsoft.2022.105436>, 2022.
- Jin, W., Zhang, W., Hu, J., Weng, B., Huang, T., and Chen, J.: Using the residual network module to correct the sub-seasonal high temperature forecast, *Front. Earth Sci.*, 9, 760766, <https://doi.org/10.3389/feart.2021.760766>, 2022.
- Kim, H., Ham, Y.-G., Joo, Y.-S., and Son, S.-W.: Deep learning for bias correction of MJO prediction, *Nat. Commun.*, 12, 3087, <https://doi.org/10.1038/s41467-021-23406-3>, 2021.
- Kim, T., Yang, T., Zhang, L., and Hong, Y.: Near real-time hurricane rainfall forecasting using convolutional neural network models with Integrated Multi-satellitE Retrievals for GPM (IMERG) product, *Atmos. Res.*, 270, 106037, <https://doi.org/10.1016/j.atmosres.2022.106037>, 2022.
- Kisi, O.: Streamflow forecasting using different artificial neural network algorithms, *J. Hydrol. Eng.*, 12, 532–539, [https://doi.org/10.1061/\(ASCE\)1084-0699\(2007\)12:5\(532\)](https://doi.org/10.1061/(ASCE)1084-0699(2007)12:5(532)), 2007.
- Kratzert, F., Klotz, D., Brenner, C., Schulz, K., and Herrnegger, M.: Rainfall–runoff modelling using Long Short-Term Memory (LSTM) networks, *Hydrol. Earth Syst. Sci.*, 22, 6005–6022, <https://doi.org/10.5194/hess-22-6005-2018>, 2018.
- Kratzert, F., Klotz, D., Herrnegger, M., Sampson, A. K., Hochreiter, S., and Nearing, G. S.: Toward improved predictions in ungauged basins: Exploiting the power of machine learning, *Water Resour. Res.*, 55, 11344–11354, <https://doi.org/10.1029/2019WR026065>, 2019.
- Kratzert, F., Gauch, M., Nearing, G., and Klotz, D.: NeuralHydrology – A Python library for Deep Learning research in hydrology, *J. Open Source Softw.*, 7, 4050, <https://doi.org/10.21105/joss.04050>, 2022 (code available at: <https://neuralhydrology.readthedocs.io/en/latest/index.html>, last access: 1 July 2024).
- Lagerquist, R., McGovern, A., and Gagne, D. J., II: Deep learning for spatially explicit prediction of synoptic-scale Fronts, *Weather Forecast.*, 34, 1137–1160, <https://doi.org/10.1175/WAF-D-18-0183.1>, 2019.
- Lam, R., Sanchez-Gonzalez, A., Willson, M., Wirnsberger, P., Fortunato, M., Alet, F., Ravuri, S., Ewalds, T., Eaton-Rosen, Z., Hu, W., Merose, A., Hoyer, S., Holland, G., Vinyals, O., Stott, J., Pritzel, A., Mohamed, S., and Battaglia, P.: Learning skillful medium-range global weather forecasting, *Science*, 382, 1416–1421, <https://doi.org/10.1126/science.adi2336>, 2023.
- Larraondo, P. R., Renzullo, L. J., Van Dijk, A. I., Inza, I., and Lozano, J. A.: Optimization of deep learning precipitation models using categorical binary metrics, *J. Adv. Model. Earth Sy.*, 12, e2019MS001909, <https://doi.org/10.1029/2019MS001909>, 2020.
- Li, J., Li, L., Zhang, T., Xing, H., Shi, Y., Li, Z., Wang, C., and Liu, J.: Flood forecasting based on radar precipitation nowcasting using U-net and its improved models, *J. Hydrol.*, 632, 130871, <https://doi.org/10.1016/j.jhydrol.2024.130871>, 2024a.
- Li, L., Yun, Z., Liu, Y., Wang, Y., Zhao, W., Kang, Y., and Gao, R.: Improving Categorical and Continuous Accuracy of Precipitation Forecasts by Integrating Empirical Quantile Mapping and Bernoulli-Gamma-Gaussian Distribution, *Atmos. Res.*, 298, 107133, <https://doi.org/10.1016/j.atmosres.2023.107133>, 2024b.
- Li, W., Pan, B., Xia, J., and Duan, Q.: Convolutional neural network-based statistical post-processing of ensemble precipitation forecasts, *J. Hydrol.*, 605, 127301, <https://doi.org/10.1016/j.jhydrol.2021.127301>, 2022.
- Li, X., Wu, H., Nanding, N., Chen, S., Hu, Y., and Li, L.: Statistical Bias Correction of Precipitation Forecasts Based on Quantile Mapping on the Sub-Seasonal to Seasonal Scale, *Remote Sens.*, 15, 1743, <https://doi.org/10.3390/rs15071743>, 2023.
- Liang, P., Lin, H., and Ding, Y.: Dominant modes of subseasonal variability of East Asian summertime surface air temperature and their predictions, *J. Climate*, 31, 2729–2743, <https://doi.org/10.1175/JCLI-D-17-0368.1>, 2018.
- Ling, F., Li, Y., Luo, J.-J., Zhong, X., and Wang, Z.: Two deep learning-based bias-correction pathways improve summer precipitation prediction over China, *Environ. Res. Lett.*, 17, 124025, <https://doi.org/10.1088/1748-9326/aca68a>, 2022a.
- Ling, F., Luo, J.-J., Li, Y., Tang, T., Bai, L., Ouyang, W., and Yamagata, T.: Multi-task machine learning improves multi-seasonal prediction of the Indian Ocean Dipole, *Nat. Commun.*, 13, 7681, <https://doi.org/10.1038/s41467-022-35412-0>, 2022b.
- Liu, D., Jiang, W., Mu, L., and Wang, S.: Streamflow prediction using deep learning neural network: case study of Yangtze River, *IEEE Access*, 8, 90069–90086, <https://doi.org/10.1109/ACCESS.2020.2993874>, 2020.
- Liu, J., Yuan, X., Zeng, J., Jiao, Y., Li, Y., Zhong, L., and Yao, L.: Ensemble streamflow forecasting over a cascade reservoir catchment with integrated hydrometeorological modeling and machine learning, *Hydrol. Earth Syst. Sci.*, 26, 265–278, <https://doi.org/10.5194/hess-26-265-2022>, 2022.
- Lyu, Y., Zhu, S., Zhi, X., Ji, Y., Fan, Y., and Dong, F.: Improving subseasonal-to-seasonal prediction of summer extreme precipitation over southern China based on a deep learning method, *Geophys. Res. Lett.*, 50, e2023GL106245, <https://doi.org/10.1029/2023GL106245>, 2023.
- Manzanas, R., Lucero, A., Weisheimer, A., and Gutiérrez, J. M.: Can bias correction and statistical downscaling methods improve the skill of seasonal precipitation forecasts?, *Clim. Dynam.*, 50, 1161–1176, <https://doi.org/10.1007/s00382-017-3669-y>, 2018.
- Mao, G., Vogl, S., Laux, P., Wagner, S., and Kunstmann, H.: Stochastic bias correction of dynamically downscaled precipitation fields for Germany through Copula-based integration of gridded observation data, *Hydrol. Earth Syst. Sci.*, 19, 1787–1806, <https://doi.org/10.5194/hess-19-1787-2015>, 2015.
- Maraun, D., Wetterhall, F., Ireson, A. M., Chandler, R. E., Kendon, E. J., Widmann, M., Brienen, S., Rust, H. W., Sauter, T., The-

- meßl, M., Venema, V. K. C., Chun, K. P., Goodess, C. M., Jones, R. G., Onof, C., Vrac, M., and Thiele-Eich, I.: Precipitation downscaling under climate change: Recent developments to bridge the gap between dynamical models and the end user, *Rev. Geophys.*, 48, RG3003, <https://doi.org/10.1029/2009RG000314>, 2010.
- Merino, A., García-Ortega, E., Navarro, A., Sánchez, J. L., and Tapiador, F. J.: WRF hourly evaluation for extreme precipitation events, *Atmos. Res.*, 274, 106215, <https://doi.org/10.1016/j.atmosres.2022.106215>, 2022.
- Michalek, A. T., Villarini, G., and Kim, T.: Understanding the impact of precipitation bias-correction and statistical downscaling methods on projected changes in flood extremes, *Earth's Future*, 12, e2023EF004179, <https://doi.org/10.1029/2023EF004179>, 2024.
- Ni, L., Wang, D., Singh, V. P., Wu, J., Chen, X., Tao, Y., Zhu, X., Jiang, J., and Zeng, X.: Monthly precipitation prediction at regional scale using deep convolutional neural networks, *Hydrol. Process.*, 37, e14954, <https://doi.org/10.1002/hyp.14954>, 2023.
- Nie, Y. and Sun, J.: Improving dynamical-statistical subseasonal precipitation forecasts using deep learning: A case study in Southwest China, *Environ. Res. Lett.*, 19, 044032, <https://doi.org/10.1088/1748-9326/ad5370>, 2024.
- Nooni, I. K., Tan, G., Hongming, Y., Chaibou, A. A. S., Habtemicheal, B. A., Gnitou, G. T., and Lim Kam Sian, K. T. C.: Assessing the performance of WRF Model in simulating heavy precipitation events over East Africa using satellite-based precipitation product, *Remote Sens.*, 14, 1964, <https://doi.org/10.3390/rs14091964>, 2022.
- Peng, T., Zhi, X., Ji, Y., Ji, L., and Tian, Y.: Prediction skill of extended range 2-m maximum air temperature probabilistic forecasts using machine learning postprocessing methods, *Atmosphere*, 11, 805, <https://doi.org/10.3390/atmos11080805>, 2020.
- Rafferty, A. E., Gneiting, T., Balabdaoui, F., and Polakowski, M.: Using Bayesian model averaging to calibrate forecast ensembles, *Mon. Weather Rev.*, 133, 1155–1174, <https://doi.org/10.1175/MWR2906.1>, 2005.
- Rasp, S. and Lerch, S.: Neural networks for postprocessing ensemble weather forecasts, *Mon. Weather Rev.*, 146, 3885–3900, <https://doi.org/10.1175/MWR-D-18-0187.1>, 2018.
- Robertson, D. E. and Wang, Q. J.: Seasonal forecasts of unregulated inflows into the Murray River, Australia, *Water Resour. Manag.*, 27, 2747–2769, <https://doi.org/10.1007/s11269-013-0313-4>, 2013.
- Sachindra, D. A., Ahmed, K., Rashid, M. M., Shahid, S., and Perera, B. J. C.: Statistical downscaling of precipitation using machine learning techniques, *Atmos. Res.*, 212, 240–258, <https://doi.org/10.1016/j.atmosres.2018.05.022>, 2018.
- Scheuerer, M. and Hamill, T. M.: Statistical post-processing of ensemble precipitation forecasts by fitting censored, shifted gamma distributions, *Mon. Weather Rev.*, 143, 4578–4596, <https://doi.org/10.1175/MWR-D-15-0061.1>, 2015.
- Shi, X.: Enabling smart dynamical downscaling of extreme precipitation events with machine learning, *Geophys. Res. Lett.*, 47, e2020GL090309, <https://doi.org/10.1029/2020GL090309>, 2020.
- Singhal, A., Jaseem, M., and Jha, S. K.: Spatial connections in extreme precipitation events obtained from NWP forecasts: A complex network approach, *Atmos. Res.*, 282, 106538, <https://doi.org/10.1016/j.atmosres.2022.106538>, 2023.
- Srivastava, A. K., Ullrich, P. A., Rastogi, D., Vahmani, P., Jones, A., and Grotjahn, R.: Assessment of WRF (v 4.2.1) dynamically downscaled precipitation on subdaily and daily timescales over CONUS, *Geosci. Model Dev.*, 16, 3699–3722, <https://doi.org/10.5194/gmd-16-3699-2023>, 2023.
- Sun, L. and Lan, Y.: Statistical downscaling of daily temperature and precipitation over China using deep learning neural models: Localization and comparison with other methods, *Int. J. Climatol.*, 41, 1128–1147, <https://doi.org/10.1002/joc.6769>, 2021.
- Sun, Q., Miao, C., Duan, Q., Ashouri, H., Sorooshian, S., and Hsu, K. L.: A review of global precipitation data sets: Data sources, estimation, and intercomparisons, *Rev. Geophys.*, 56, 79–107, <https://doi.org/10.1002/2014RG000477>, 2016.
- Tabari, H., Paz, S. M., Buekenhout, D., and Willems, P.: Comparison of statistical downscaling methods for climate change impact analysis on precipitation-driven drought, *Hydrol. Earth Syst. Sci.*, 25, 3493–3517, <https://doi.org/10.5194/hess-25-3493-2021>, 2021.
- Taillardat, M., Mestre, O., Zamo, M., and Naveau, P.: Calibrated ensemble forecasts using quantile regression forests and ensemble model output statistics, *Mon. Weather Rev.*, 144, 2375–2393, <https://doi.org/10.1175/MWR-D-15-0260.1>, 2016.
- Tan, Y., Dong, N., Hou, A., and Yan, W.: An improved Xin'anjiang hydrological model for flood simulation coupling snowmelt runoff module in Northwestern China, *Water*, 15, 3401, <https://doi.org/10.3390/w15193401>, 2023.
- Valdez, E. S., Anctil, F., and Ramos, M.-H.: Choosing between post-processing precipitation forecasts or chaining several uncertainty quantification tools in hydrological forecasting systems, *Hydrol. Earth Syst. Sci.*, 26, 197–220, <https://doi.org/10.5194/hess-26-197-2022>, 2022.
- Vandal, T., Kodra, E., and Ganguly, A. R.: Intercomparison of machine learning methods for statistical downscaling: the case of daily and extreme precipitation, *Theor. Appl. Climatol.*, 137, 557–570, <https://doi.org/10.1007/s00704-018-2613-3>, 2019.
- Vigaud, N., Tippett, M. K., and Robertson, A. W.: Deterministic skill of subseasonal precipitation forecasts for the East Africa-West Asia sector from September to May, *J. Geophys. Res.-Atmos.*, 124, 11887–11896, <https://doi.org/10.1029/2019JD030747>, 2019.
- Vrac, M. and Friederichs, P.: Multivariate-intervariable, spatial, and temporal bias correction, *J. Climate*, 28, 218–237, <https://doi.org/10.1175/JCLI-D-14-00059.1>, 2015.
- Wang, R., Zhang, J., Guo, E., Zhao, C., and Cao, T.: Spatial and temporal variations of precipitation concentration and their relationships with large-scale atmospheric circulations across Northeast China, *Atmos. Res.*, 222, 62–73, <https://doi.org/10.1016/j.atmosres.2019.02.008>, 2019.
- Wei, L., Hu, K.-H., and Hu, X.-D.: Rainfall occurrence and its relation to flood damage in China from 2000 to 2015, *J. Mt. Sci.*, 15, 2492–2504, <https://doi.org/10.1007/s11629-018-4931-4>, 2018.
- Weyn, J. A., Durran, D. R., Caruana, R., and Cresswell-Clay, N.: Sub-seasonal forecasting with a large ensemble of deep-learning weather prediction models, *J. Adv. Model. Earth Sy.*, 13, e2021MS002502, <https://doi.org/10.1029/2021MS002502>, 2021.
- Xie, J., Hsu, P.-C., Hu, Y., Ye, M., and Yu, J.: Skillful extended-range forecast of rainfall and extreme events in East China

- based on deep learning, *Weather Forecast.*, 38, 467–486, <https://doi.org/10.1175/WAF-D-22-0132.1>, 2023.
- Xu, Y. P., Gao, X., Zhu, Q., and Zhang, Y.: Coupling a regional climate model and distributed hydrological model to assess future water resources in Jinhua River Basin, East China, *J. Hydrol. Eng.*, 20, 04014054, [https://doi.org/10.1061/\(ASCE\)HE.1943-5584.0001007](https://doi.org/10.1061/(ASCE)HE.1943-5584.0001007), 2015.
- Yang, S., Yang, D., Chen, J., Santisirisomboon, J., and Zhao, B.: A physical process and machine learning combined hydrological model for daily streamflow simulations of large watersheds with limited observation data, *J. Hydrol.*, 590, 125206, <https://doi.org/10.1016/j.jhydrol.2020.125206>, 2020.
- You, X. X., Liang, Z. M., Wang, Y. Q., and Zhang, H.: A study on loss function against data imbalance in deep learning correction of precipitation forecasts, *Atmos. Res.*, 281, 106500, <https://doi.org/10.1016/j.atmosres.2022.106500>, 2023.
- Yuan, X., Wood, E. F., Luo, L., and Pan, M.: A first look at Climate Forecast System version 2 (CFSv2) for hydrological seasonal prediction, *Geophys. Res. Lett.*, 38, L13401, <https://doi.org/10.1029/2011GL047792>, 2011.
- Yuan, X., Ma, F., Wang, L., Zheng, Z., Ma, Z., Ye, A., and Peng, S.: An experimental seasonal hydrological forecasting system over the Yellow River basin – Part 1: Understanding the role of initial hydrological conditions, *Hydrol. Earth Syst. Sci.*, 20, 2437–2451, <https://doi.org/10.5194/hess-20-2437-2016>, 2016.
- Yuan, X., Wang, S., and Hu, Z.-Z.: Do climate change and El Niño increase likelihood of Yangtze River extreme rainfall?, *B. Am. Meteorol. Soc.*, 99, S113–S117, <https://doi.org/10.1175/BAMS-D-17-0089.1>, 2018.
- Zhang, Q., Li, Y. P., Huang, G. H., Wang, H., Li, Y. F., Liu, Y. R., and Shen, Z. Y.: A novel statistical downscaling approach for analyzing daily precipitation and extremes under the impact of climate change: Application to an arid region, *J. Hydrol.*, 615, 128730, <https://doi.org/10.1016/j.jhydrol.2022.128730>, 2022a.
- Zhang, T., Liang, Z., Li, W., Wang, J., Hu, Y., and Li, B.: Statistical post-processing of precipitation forecasts using circulation classifications and spatiotemporal deep neural networks, *Hydrol. Earth Syst. Sci.*, 27, 1945–1960, <https://doi.org/10.5194/hess-27-1945-2023>, 2023.
- Zhang, Y., Ragetti, S., Molnar, P., Fink, O., and Peleg, N.: Generalization of an Encoder-Decoder LSTM model for flood prediction in ungauged catchments, *J. Hydrol.*, 614, 128577, <https://doi.org/10.1016/j.jhydrol.2022.128577>, 2022b.
- Zhao, R. J.: The Xin’anjiang model applied in China, *J. Hydrol.*, 135, 371–381, [https://doi.org/10.1016/0022-1694\(92\)90096-E](https://doi.org/10.1016/0022-1694(92)90096-E), 1992.
- Zhu, E., Yuan, X., and Wood, A.: Benchmark decadal forecast skill for terrestrial water storage estimated by an elasticity framework, *Nat. Commun.*, 10, 1237, <https://doi.org/10.1038/s41467-019-09245-3>, 2019.
- Zhu, S., Remedio, A. R. C., Sein, D. V., Sielmann, F., Ge, F., Xu, J., Peng, T., Jacob, D., Zhi, X., and Fraedrich, K.: Added value of the regionally coupled model ROM in the East Asian summer monsoon modeling, *Theor. Appl. Climatol.*, 140, 375–387, <https://doi.org/10.1007/s00704-020-03093-8>, 2020.